

# Graph-based Square-Root Estimation for Sparse Linear Regression

Peili Li <sup>\*</sup>    Zhuomei Li <sup>†</sup>    Yunhai Xiao <sup>‡</sup>    Chao Ying <sup>§</sup>    Zhou Yu <sup>¶</sup>

## Abstract

Sparse linear regression is one of the classic problems in the field of statistics, which has deep connections and high intersections with optimization, computation, and machine learning. To address the effective handling of high-dimensional data, the diversity of real noise, and the challenges in estimating standard deviation of the noise, we propose a novel and general graph-based square-root estimation (GSRE) model for sparse linear regression. Specifically, we use square-root-loss function to encourage the estimators to be independent of the unknown standard deviation of the error terms and design a sparse regularization term by using the graphical structure among predictors in a node-by-node form. Based on the predictor graphs with special structure, we highlight the generality by analyzing that the model in this paper is equivalent to several classic regression models. Theoretically, we also analyze the finite sample bounds, asymptotic normality and model selection consistency of GSRE method without relying on the standard deviation of error terms. In terms of computation, we employ the fast and efficient alternating direction method of multipliers. Finally, based on a large number of simulated and real data with various types of noise, we demonstrate the performance advantages of the proposed method in estimation, prediction and model selection.

**Key words.** Sparse linear regression, square-root-loss function, graphical structure among predictors, alternating direction method of multipliers, oracle property.

## 1 Introduction

A very active research area in statistics is the linear regression problem, whose classical model is often assumed as  $y = X\beta^* + \sigma\epsilon$ , where  $y \in \mathbb{R}^n$  is the observed response variable,  $X \in \mathbb{R}^{n \times p}$  is the design matrix,  $\beta^* \in \mathbb{R}^p$  is the true coefficient to be estimated,  $\sigma \geq 0$  is the noise level, and  $\epsilon \in \mathbb{R}^n$  is an error vector of i.i.d. random variables with mean zero. Many practical applications often encounter high-dimensional small-sample data, i.e., situations with small  $n$  and large  $p$ , which will lead to the phenomenon of rank deficiency in the design matrix  $X$ . Moreover, the effectiveness of traditional least squares estimation model will be greatly challenged when the predictive variables are highly correlated or the data contains non-normal distributed noise. High-dimensional statistical modeling often employs sparse penalty methods, which involves adding different penalty functions to the square loss function  $\|y - X\beta\|^2$  for variable selection, such as  $\ell_1$  penalty [41],  $L_p$  ( $0 < p < 1$ ) quasi-norm [16], smoothly clipped absolute deviation (SCAD)

<sup>\*</sup>School of Mathematics and Statistics, Henan University, Kaifeng 475000, China (Email: lipeili@henu.edu.cn).

<sup>†</sup>School of Mathematics and Statistics, Henan University, Kaifeng 475000, China (Email: zhuomeili@henu.edu.cn).

<sup>‡</sup>Corresponding author. Center for Applied Mathematics of Henan Province, Henan University, Zhengzhou 450046, China (Email: yhxiao@henu.edu.cn).

<sup>§</sup>Department of Biostatistics and Medical Informatics, University of Wisconsin-Madison, Madison, WI 53726, USA (Email: cying8@wisc.edu).

<sup>¶</sup>School of Statistics, East China Normal University, Shanghai 200062, China (Email: zyu@stat.ecnu.edu.cn).

[14], minimax concave penalty (MCP) [53], etc. In addition, in some practical problems, such as sparse kernel learning [24], additive modeling [33] and multivariate regression [17], variable selection needs to be performed in the form of groups, which has led to the development of group penalty methods, such as group lasso [7, 51]. However, its obvious limitation lies in the non-overlapping structure, which makes it unsuitable for the practical problems where features may be encoded in multiple groups, such as many biological studies on gene interactions [29, 39].

To address the aforementioned issues, we have noticed that some literature have utilized the connectivity of an undirected graph to simulate the structural information among the predictors and improve sparse regression models based on this graph. Early literature mostly used edge-by-edge method, which employs penalty functions to promote similarity in regression coefficients for correlated predictors [5, 23, 29, 49]. However, these methods did not directly utilize the neighborhood information of the graph. Additionally, when there are more edges in the graph, this approach leads to more complex penalty terms. As an improvement, [50] proposed a node-wise penalty by using a node-by-node method. Specifically, given the predictor graph  $G$  and positive weights  $\tau_i$ 's, they defined the following norm

$$\|\beta\|_{G,\tau} = \min_{\sum_{i=1}^p V^{(i)} = \beta, \text{supp}(V^{(i)}) \subseteq \mathcal{N}_i} \sum_{i=1}^p \tau_i \|V^{(i)}\|_2, \quad (1.1)$$

where  $\text{supp}(V^{(i)})$  is the support of vector  $V^{(i)} \in \mathbb{R}^p$ ,  $\|\cdot\|_2$  is the  $\ell_2$  norm, and  $\mathcal{N}_i$  represents the set containing the predictor  $i$  and its neighbors in graph  $G$ . They no longer focus on the original variable  $\beta$  of the model, but decompose  $\beta$  into  $p$  parts, and then use group sparsity idea based on predictor graph information. This design motivation comes from the explicit expression between the true coefficient and the inverse covariance matrix in analyzing least squares estimation. With the above notation, their optimization model in sparse regression incorporating graphical structure among predictors (SRIG) is given by

$$\min_{\beta \in \mathbb{R}^p} \left\{ \frac{\|y - X\beta\|_2^2}{2n} + \lambda \|\beta\|_{G,\tau} \right\}, \quad (1.2)$$

where  $\lambda$  is a regularization parameter. The SRIG method facilitates the inclusion of other predictors connected to an important predictor in a model, which is better suited to meet the demands of practical applications. Compared to penalty methods that do not use the graphical structure among predictors, SRIG method can significantly improve the performance of variable selection, estimation and prediction. The good performance of this research idea has attracted the attention of many scholars and has been extended to linear discriminant analysis [30], generalized linear regression [32, 38, 56], expectile regression [36], quantile regression [46], etc.

Despite these attractive features, there still exists a theoretical and practical challenge. Because the aforementioned problems based on the smooth square loss usually need to assume that the noise follows a normal distribution, and the estimation performance depends on knowing standard deviation of the error terms in advance. The theoretical form of the regularization parameter  $\lambda$ , which is crucial for the model estimation, relies on the standard deviation  $\sigma$ . However, in high-dimensional settings, accurately estimating  $\sigma$  is a non-trivial task, and the types of noise generally exhibit diversity. Fortunately, the proposal of the square-root-loss function overcomes the aforementioned limitations, which was first proposed by [35]. Based on the idea of square-root loss, [3] extended the traditional lasso problem and obtained the following square-root lasso (SRL):

$$\min_{\beta \in \mathbb{R}^p} \left\{ \frac{\|y - X\beta\|_2}{\sqrt{n}} + \frac{\lambda}{n} \|\beta\|_1 \right\}, \quad (1.3)$$

where  $\|\beta\|_1 = \sum_{i=1}^p |\beta_i|$  is the  $\ell_1$  norm of  $\beta$ . It has been theoretically validated that SRL can achieve

near-oracle property without knowing or estimating  $\sigma$  in advance. This makes the lasso-type methods much more attractive in high-dimensional scenarios. Subsequently, the square-root loss was shown to be applicable to non-normal noise under reasonable conditions [2, 11]. Furthermore, [8] extended the ideas behind the SRL for group selection. [40] proposed a nonconvex square-root-loss regression model. For more research on the square-root-loss function, one can refer to [12, 13, 37].

In this paper, we carry out research on integrating the square-root-loss regression method and the penalty methods based on graphical structure among predictors. This research aims to construct a novel model for the classic high-dimensional linear regression problem, which can analyze the intrinsic information in data and alleviate the reliance on normal noise. Specifically, we propose the following graph-based square-root estimation (GSRE) model:

$$\min_{\beta \in \mathbb{R}^p} \left\{ \frac{\|y - X\beta\|_2}{\sqrt{n}} + \frac{\lambda}{n} \|\beta\|_{G,\tau} \right\}. \quad (1.4)$$

To the best of our knowledge, this is the first time that square-root-loss regression incorporating graphical structure among predictors. Firstly, for several classes of predictor graphs with special structures, we verify the equivalence of the proposed GSRE method with several existing methods. Then, when the graphical structure  $G$  of the predictors is known, we provide finite sample bounds, asymptotic normality and model selection consistency for the GSRE method with a  $\sigma$ -free tuning sequence  $\lambda$ . For the case where the graphical structure  $G$  is unknown, we construct it by sparse estimating the covariance (or precision) matrix of the predictors [9, 18, 52]. In terms of computation, we adopt the classical alternating direction method of multipliers (ADMM) in the optimization field. Simulation studies and practical applications demonstrate that the proposed GSRE method exhibits good performance in variable selection, model estimation and prediction.

**Organization:** The remainder of this paper is organized as follows. Relevant and rigorous theoretical results are presented in Section 2. Section 3 provides a detailed description of the classical ADMM for model (1.4). Section 4 demonstrates the numerical performance of the proposed GSRE method on both simulated and real data. Finally, we summarize this paper in Section 5.

**Notation:** To end this section, we summarize some notations used in this paper.  $[p] := \{1, 2, \dots, p\}$ . When  $|\cdot|$  is applied to a scalar, it denotes the absolute value, and when it acts on a set, it denotes the cardinality. For each  $i \in [p]$ , we denote  $d_i$  as the number of predictors in the neighborhood  $\mathcal{N}_i$ , that is,  $d_i = |\mathcal{N}_i|$ .  $d_{min} := \min_{1 \leq i \leq p} d_i$ ,  $d_{max} := \max_{1 \leq i \leq p} d_i$ ,  $\tau_{min} := \min_{1 \leq i \leq p} \tau_i$ . For each  $i \in [p]$ , denote  $\zeta_i = \|X_{\mathcal{N}_i}\|^2$  and  $\zeta = \max_i \zeta_i$ , where  $\|X_{\mathcal{N}_i}\|$  is the operator norm of the matrix  $X_{\mathcal{N}_i}$ . For a  $n \times p$  matrix  $M$ ,  $\|M\|_\infty$  is defined as  $\max_{1 \leq i \leq n} \sum_{j=1}^p |M_{ij}|$ . For a constant  $x$ , we denote  $(x)_+ = \max(x, 0)$ . Here, we denote  $\mathcal{I}_* := \{i : \beta_i^* \neq 0\}$ ,  $\mathcal{I}_*^c := \{i : \beta_i^* = 0\}$  and  $s^* = |\mathcal{I}_*|$  as the true nonzero coefficient set, the true zero coefficient set, and the number of true nonzero coefficients, respectively. For every  $\beta \in \mathcal{R}^p$ , denote  $\beta_{\mathcal{I}_*}$  and  $\beta_{\mathcal{I}_*^c}$  as the subvectors of  $\beta$  with indices in  $\mathcal{I}_*$  and  $\mathcal{I}_*^c$  respectively. For any matrix  $M$ ,  $M_{\mathcal{I}_*, \mathcal{I}_*}$  denote the submatrix of  $M$  consisting of the entries with row and column indices in  $\mathcal{I}_*$ .  $\beta_{min}^* = \min_{i \in \mathcal{I}_*} |\beta_i^*|$  denote the minimum absolute nonzero coefficient.  $\text{sign}(\cdot)$  maps a positive entry to 1, a negative entry to  $-1$ , and zero to zero. The symbol  $\delta_{\mathcal{C}}(x)$  represents the indicator function over  $\mathcal{C}$  such that  $\delta_{\mathcal{C}}(x) = 0$  if  $x \in \mathcal{C}$  and  $+\infty$  otherwise.

## 2 Theoretical results

In this section, we will give some relevant and rigorous theoretical results with a non-random design matrix. Specifically, we first characterize the features of optimal solution by analyzing the subgradient conditions of GSRE problem. Then, based on the given predictor graphs with certain special structures, we establish the connections between the proposed GSRE model and several other existing penalized

problems. Subsequently, we analyze the finite sample bounds, asymptotic normality and model selection consistency of the GSRE method with a  $\sigma$ -free tuning sequence  $\lambda$ .

## 2.1 Subgradient conditions

**Lemma 2.1.** *Assume there exists a vector  $\beta \in \mathbb{R}^p$  satisfying  $X\beta \neq y$ . Then  $\beta$  is an optimal solution of (1.4) if and only if  $\beta$  can be decomposed as  $\beta = \sum_{i=1}^p V^{(i)}$  where  $V^{(i)}$ 's satisfy that, for all  $1 \leq i \leq p$ ,*

(a)  $V_{\mathcal{N}_i^c}^{(i)} = 0$ ;

(b) either  $V_{\mathcal{N}_i}^{(i)} \neq 0$  and  $\frac{X_{\mathcal{N}_i}^\top (y - X\beta)}{\|y - X\beta\|_2} = \frac{\lambda \tau_i V_{\mathcal{N}_i}^{(i)}}{\sqrt{n} \|V_{\mathcal{N}_i}^{(i)}\|_2}$ , or  $V_{\mathcal{N}_i}^{(i)} = 0$  and  $\frac{\|X_{\mathcal{N}_i}^\top (y - X\beta)\|_2}{\|y - X\beta\|_2} \leq \frac{\lambda \tau_i}{\sqrt{n}}$ .

*Proof.* See Appendix A. □

**Remark 2.1.** *According to Lemma 2.1, if  $(\hat{V}^{(1)}, \hat{V}^{(2)}, \dots, \hat{V}^{(p)})$  is a decomposition of the optimal solution of (1.4), then for each  $i$ , either  $\hat{V}^{(i)} = \mathbf{0}_p$  or  $\text{supp}(\hat{V}^{(i)}) = \mathcal{N}_i$ . This result is very consistent with the design idea of node-wise penalty.*

## 2.2 Connections with some existing methods

**Lemma 2.2.** (a) *If the predictor graph has no edge, the problem (1.4) is the same as*

$$\min_{\beta \in \mathbb{R}^p} \left\{ \frac{\|y - X\beta\|_2}{\sqrt{n}} + \frac{\lambda}{n} \sum_{i=1}^p \tau_i |\beta_i| \right\}. \quad (2.1)$$

When  $\tau_i \equiv 1$  for each  $i$ , (2.1) is the classic square-root lasso [3].

(b) *If the predictor graph consists of  $J$  disconnected complete subgraphs, and the nodes in the  $J$  disconnected complete subgraphs are assumed to be  $\{1, 2, \dots, q_1\}, \{q_1 + 1, \dots, q_1 + q_2\}, \dots, \{q_{J-1} + 1, \dots, q_{J-1} + q_J\}$ , then the problem (1.4) is equivalent to*

$$\min_{\beta \in \mathbb{R}^p} \left\{ \frac{\|y - X\beta\|_2}{\sqrt{n}} + \frac{\lambda}{n} \sum_{j=1}^J \tilde{\tau}_j \|\beta^{(j)}\|_2 \right\}, \quad (2.2)$$

where  $\tilde{\tau}_j = \min_{q_{j-1}+1 \leq i \leq q_{j-1}+q_j} \tau_i$  and  $\beta^{(j)} = (\beta_{q_{j-1}+1}, \beta_{q_{j-1}+2}, \dots, \beta_{q_{j-1}+q_j})^\top$ . Obviously, this problem is exactly the group square-root lasso problem [8].

(c) *If the predictor graph is a complete graph, then the problem (1.4) has the same nonzero solutions as*

$$\min_{\beta \in \mathbb{R}^p} \left\{ \frac{\|y - X\beta\|_2}{\sqrt{n}} + \frac{\tilde{\lambda}}{n} \|\beta\|_2^2 \right\}, \quad (2.3)$$

where  $\tilde{\lambda}$  is a tuning parameter different from  $\lambda$ .

*Proof.* See Appendix B. □

**Remark 2.2.** *Lemma 2.2 shows that square-root lasso and group square-root lasso are special cases of the proposed model (1.4). This conclusion validates the broader applicability of our model, enabling it to handle predictor graphs with diverse structures.*

## 2.3 Choice of the tuning parameter

As is well known, accurately estimating the unknown standard deviation  $\sigma$  of noise is very challenging in high-dimensional settings. In this part, we will use the ratio of random variables to determine the choice of the tuning parameter  $\lambda$ , thus removing the dependence on  $\sigma$ . Specifically, for any predictor graph  $G$ , we define

$$V := \max_{1 \leq i \leq p} \left\{ \frac{\sqrt{n} \|X_{\mathcal{N}_i}^\top \epsilon\|_2}{\tau_i \|\epsilon\|_2} \right\}.$$

For a given constant  $r > 1$ , we set  $\bar{r} := \frac{r+1}{r-1}$ . For given  $\lambda > 0$ , we define the set

$$\mathcal{A} := \{V \leq \lambda/\bar{r}\}. \quad (2.4)$$

Next, we will prove that, for any  $\alpha$  close to zero and a suitable tuning parameter  $\lambda$ , the set  $\mathcal{A}$  holds with probability  $1 - \alpha$ . Before presenting the specific conclusion, we first provide the following assumption:

**Assumption 2.1.** *The additive noise terms  $\epsilon_i$  follow a standard Gaussian distribution.*

**Lemma 2.3.** *Assumption 2.1 is satisfied and  $0 < d_i < n$  for all  $1 \leq i \leq p$ . Let  $\alpha \in (0, 1)$  be given such that  $16 \log(2p/\alpha) \leq n - d_{\max}$ . Then if we choose a parameter  $\lambda$  that satisfies*

$$\lambda \geq \frac{n\bar{r}\sqrt{2\zeta d_{\max}}}{\tau_{\min}\sqrt{n-d_{\max}}} \left(1 + \sqrt{\frac{2\log(2p/\alpha)}{d_{\min}}}\right), \quad (2.5)$$

it holds that  $\mathbb{P}(V \leq \frac{\lambda}{\bar{r}}) \geq 1 - \alpha$ .

*Proof.* See Appendix C. □

**Remark 2.3.** *Based on  $d_i = |\mathcal{N}_i|$ , for any  $i$ , we can have  $d_i \geq 1$ . Additionally, since we are concerned with sparsity issues, it is a common assumption that the number of mutually related predictors in the predictor graph is less than  $n$ . An immediate consequence of this lemma is that, for any given  $\alpha$  approaching 0, a  $\sigma$ -free expression of  $\lambda$  holds with probability  $1 - \alpha$ , which is a very important additional benefit.*

**Remark 2.4.** *It can be noted that the analysis in this part only considers Gaussian noise, but the results can also be generalized to different types of noise by applying different deviation inequalities [6, 27, 42]. For example, if  $\epsilon_i$ 's belong to a general sub-exponential family, the order of magnitude of  $\lambda$  remains the same. For more analysis on non-Gaussian noise, one can refer to [3]. A detailed study is omitted here.*

## 2.4 Finite sample bounds

In this subsection, we will give the results of finite sample bounds for the proposed GSRE method over the set  $\mathcal{A}$ . The following assumptions need to be considered in subsequent analysis.

**Assumption 2.2.** *The neighborhood  $\mathcal{N}_i \subseteq \mathcal{I}_*$  for each  $i \in \mathcal{I}_*$ .*

**Assumption 2.3.** *For a subset  $J \subset [p]$ , there exists  $\kappa > 0$  and  $r > 1$  such that*

$$\sum_{i \in J} \tau_i \|V^{(i)}\|_2 \leq \frac{\sqrt{s^*} \|X\beta\|_2}{\sqrt{n\kappa}}$$

for all  $(V^{(1)}, V^{(2)}, \dots, V^{(p)}) \in \mathcal{T}_{G,\tau}(\beta, J)$ , where  $\mathcal{T}_{G,\tau}(\beta, J)$  is the set of all optimal decompositions of  $\beta$  such that

$$\sum_{i \in J^c} \tau_i \|V^{(i)}\|_2 \leq r \sum_{i \in J} \tau_i \|V^{(i)}\|_2.$$

**Assumption 2.4.** The number of true nonzero coefficients  $s^*$  satisfies  $s^* < \frac{n^2 \kappa^2}{\lambda^2}$ .

**Remark 2.5.** Assumption 2.2 guarantees that predictors connected to the useful predictors are also useful, which is reasonable. Assumption 2.3 is a general compatibility condition on the design matrix [7, 8] and is a slight relaxation of the widely used restricted eigenvalue condition [4]. The constant  $\kappa$  quantifies the correlations in the design matrix: a smaller value of  $\kappa$  indicates stronger correlations. Assumption 2.4 essentially constrains the true model to have fewer parameters than  $n$ .

**Theorem 2.1.** Assumptions 2.1, 2.2, 2.3, 2.4 hold. Then, on the event  $\mathcal{A}$ , for any optimal solution  $\hat{\beta}$  of model (1.4), we have

$$\frac{\|X(\hat{\beta} - \beta^*)\|_2}{\sqrt{n}} \lesssim \frac{\sigma \lambda \sqrt{s^*}}{n \kappa}, \quad \|\hat{\beta} - \beta^*\|_{G, \tau} \lesssim \frac{\sigma \lambda s^*}{n \kappa^2}, \quad \|\hat{\beta} - \beta^*\|_2 \lesssim \frac{\sigma \lambda s^*}{n \kappa^2 \tau_{\min}},$$

with probability at least  $1 - (1 + e^2)e^{-n/24}$ .

*Proof.* See Appendix D. □

**Remark 2.6.** Theorem 2.1 conducts an estimation analysis based on a tuning parameter independent of  $\sigma$  and yields results similar to existing literature related to group lasso and group square-root lasso estimators [8, 31]. Furthermore, it is noted that, from Theorem 2.1, subset recovery can be guaranteed with no noise, i.e.,  $\sigma = 0$ . However, for classical least squares methods such as lasso, elastic net and group lasso, even if  $\sigma = 0$ , accurate recovery cannot be guaranteed because their tuning parameters are heavily dependent on  $\sigma$ . Additionally, combining with Lemma 2.3 on the selection of regularization parameter, it can be concluded that the result of Theorem 2.1 holds with probability  $1 - \alpha - (1 - \alpha)(1 + e^2)e^{-n/24}$ .

## 2.5 Asymptotic normality and model selection consistency

In this subsection, we first study the asymptotic normality of the proposed GSRE method in the case where the dimension  $p$  is fixed. Then, we analyze the model selection consistency in the high-dimensional case where  $p$  grows with  $n$ . For the case of fixed  $p$ , we need the following two commonly used assumptions:

**Assumption 2.5.** As  $n \rightarrow \infty$ ,  $X^\top X/n \rightarrow M$ , where  $M$  is a positive matrix.

**Assumption 2.6.** The errors  $\epsilon_1, \epsilon_2, \dots, \epsilon_n$  are i.i.d. variables with mean 0 and variance 1.

**Theorem 2.2.** Assumptions 2.2, 2.5, 2.6 hold. Suppose that as  $n \rightarrow \infty$ , the tuning parameter  $\lambda$  is chosen such that  $\lambda/\sqrt{n} \rightarrow 0$  and  $\lambda n^{(\nu-1)/2} \rightarrow \infty$  for some  $\nu > 1$ . Furthermore,  $\tau_i = O(1)$  for each  $i \in \mathcal{I}_*$  and  $\liminf_{n \rightarrow \infty} n^{-\nu/2} \tau_i > 0$  for each  $i \in \mathcal{I}_*$ . Then, with dimension  $p$  fixed, as  $n \rightarrow \infty$ , we have

$$\sqrt{n}(\hat{\beta}_{\mathcal{I}_*} - \beta_{\mathcal{I}_*}^*) \xrightarrow{d} N(0, \sigma^2 M_{\mathcal{I}_*, \mathcal{I}_*}^{-1}), \quad \hat{\beta}_{\mathcal{I}_*^c} \xrightarrow{p} 0. \quad (2.6)$$

*Proof.* See Appendix E. □

**Remark 2.7.** Theorem 2.2 indicates that the proposed GSRE method is estimation-consistent when  $p$  is fixed. Clearly, the above result can be naturally extended to the random design setting. The relevant detailed discussion is omitted here.

**Remark 2.8.** Theorem 2.2 also provides a guideline on how to choose the positive weight  $\tau_i$ . [34] suggest to consider  $\tau_i = d_i^\eta$  for some  $\eta \in (0, \frac{1}{2})$ . More specially, they give a critical value with  $\eta = \frac{\log(2)}{2\log(3)}$ , which is the smallest value that it becomes impossible to select a support of exactly two covariates. In our numerical experiments, we also choose  $\tau_i = d_i^\eta$  with  $\eta = \frac{\log(2)}{2\log(3)}$ .

Next, we consider the high-dimensional case where the dimension  $p$  grows with  $n$ , while the design matrix  $X$  is fixed. The subsequent analysis requires the following assumptions:

**Assumption 2.7.** *The number of nonzero coefficients  $s^* = O(n^{\delta_0})$  for some constant  $\delta_0 \in (0, 1)$ .*

**Assumption 2.8.** *There exists a constant  $Q_1 > 0$  such that  $\max_{i \in \mathcal{I}_*^c} \|X_i\|_2 \leq \frac{Q_1}{\sqrt{n}}$  for each  $n$ .*

**Assumption 2.9.** *There exists a constant  $Q_2 > 0$  such that the smallest eigenvalue of  $\frac{X_{\mathcal{I}_*}^\top X_{\mathcal{I}_*}}{n}$  is larger than  $Q_2$  for each  $n$ .*

**Assumption 2.10.** *There exists a constant  $\xi \in (0, 1)$  such that  $\|X_{\mathcal{N}_i}^\top X_{\mathcal{I}_*} (X_{\mathcal{I}_*}^\top X_{\mathcal{I}_*})^{-1}\|_\infty \leq 1 - \xi$ .*

**Remark 2.9.** *Assumption 2.7 ensures the sparsity of the problem. Assumption 2.8 can be achieved by normalizing each predictor. Assumption 2.9 guarantees that matrix  $\frac{X_{\mathcal{I}_*}^\top X_{\mathcal{I}_*}}{n}$  is invertible. Assumption 2.10 is similar to the strong irrepresentable condition [55].*

**Theorem 2.3.** *Assumptions 2.1-2.4 and 2.7-2.10 hold. Suppose  $\tau_i = \sqrt{d_i} m_i$  for each  $i$ , where the  $m_i$ 's satisfy that  $\max_{i \in \mathcal{I}_*} m_i = O_p(1)$  and  $\liminf_{n \rightarrow \infty} n^{-\varsigma} \min_{i \in \mathcal{I}_*^c} m_i > 0$  for some  $\varsigma > \delta_0$ . Furthermore, as  $n \rightarrow \infty$  and  $p = p(n) \rightarrow \infty$ , the selected tuning parameter  $\lambda$  satisfy that,*

$$\frac{1}{\beta_{min}^*} \left( 3\sigma \sqrt{\frac{\log s^*}{nQ_2}} + \frac{2\sigma\lambda\sqrt{s^*}}{nQ_2} \left( 1 + \frac{C\lambda\sqrt{s^*}}{n\kappa} \right) \max_{i \in \mathcal{I}_*} \tau_i \right) \rightarrow 0 \text{ and } \frac{\sqrt{\log(p - s^*)}}{\lambda\sqrt{n} \min_{i \in \mathcal{I}_*^c} m_i} \rightarrow 0.$$

Then, on the set  $\mathcal{A}$ , as  $n \rightarrow \infty$  and  $p = p(n) \rightarrow \infty$ , there exists a solution  $\hat{\beta}$  to (1.4) such that  $\text{sign}(\hat{\beta}) = \text{sign}(\beta^*)$  with probability tending to 1.

*Proof.* See Appendix F. □

**Remark 2.10.** *Theorem 2.3 indicates that the proposed GSRE method is model selection consistent in high-dimensional settings.*

### 3 Computation

Upon careful observation, we note that model (1.4) has two non-smooth convex structures. It is well known that ADMM is a flexible and efficient optimization method that can handle convex optimization problems with separable structures and linear constraints. Therefore, we use ADMM for the computation here. First, to effectively utilize ADMM, we introduce two auxiliary variables to reformulate model (1.4) as the following minimization problem with two-block separable structures and two linear constraints:

$$\begin{aligned} \min_{\beta, u, v} \quad & \frac{\|u\|_2}{\sqrt{n}} + \frac{\lambda}{n} \|v\|_{G, \tau} \\ \text{s.t.} \quad & X\beta - u = y, \\ & \beta - v = 0. \end{aligned} \tag{3.1}$$

Given  $\sigma > 0$ , the augmented Lagrangian function of (3.1) is defined by

$$\begin{aligned} \mathcal{L}_\sigma(\beta, u, v; z, w) := & \frac{\|u\|_2}{\sqrt{n}} + \frac{\lambda}{n} \|v\|_{G, \tau} + \langle z, X\beta - u - y \rangle + \langle w, \beta - v \rangle \\ & + \frac{\sigma}{2} \|X\beta - u - y\|^2 + \frac{\sigma}{2} \|\beta - v\|^2. \end{aligned}$$

Starting from an initial point  $(u^0, v^0, z^0, w^0) \in \mathbb{R}^n \times \mathbb{R}^p \times \mathbb{R}^n \times \mathbb{R}^p$ , we use ADMM to update the variables sequentially. Specifically, with the given  $(u^k, v^k, z^k, w^k)$ , the new iteration  $(\beta^{k+1}, u^{k+1}, v^{k+1}, z^{k+1}, w^{k+1})$  is generated via the following iterative scheme:

$$\begin{cases} \beta^{k+1} = \arg \min_{\beta \in \mathbb{R}^p} \mathcal{L}_\sigma(\beta, u^k, v^k; z^k, w^k), \\ u^{k+1} = \arg \min_{u \in \mathbb{R}^n} \mathcal{L}_\sigma(\beta^{k+1}, u, v^k; z^k, w^k), \\ v^{k+1} = \arg \min_{v \in \mathbb{R}^p} \mathcal{L}_\sigma(\beta^{k+1}, u^{k+1}, v; z^k, w^k), \\ z^{k+1} = z^k + \tau\sigma(X\beta^{k+1} - u^{k+1} - y), \\ w^{k+1} = w^k + \tau\sigma(\beta^{k+1} - v^{k+1}), \end{cases}$$

where  $\tau \in (0, (1 + \sqrt{5})/2)$  is the step size. Next, we will primarily focus on solving the inner minimization subproblems.

First, for the  $\beta$ -subproblem, we can easily get

$$\begin{aligned} \beta^{k+1} &= \arg \min_{\beta \in \mathbb{R}^p} \left\{ \langle z^k, X\beta - u^k - y \rangle + \langle w^k, \beta - v^k \rangle + \frac{\sigma}{2} \|X\beta - u^k - y\|^2 + \frac{\sigma}{2} \|\beta - v^k\|^2 \right\} \\ &= \left( \mathcal{I}_p + X^\top X \right)^{-1} \left( v^k - \sigma^{-1} w^k + X^\top (u^k + y - \sigma^{-1} z^k) \right). \end{aligned}$$

In order to avoid the time-consuming issue of inverting large matrices in high-dimensional environments, we use the Sherman-Morrison-Woodbury formula [20] in specific computations, i.e.,  $\left( \mathcal{I}_p + X^\top X \right)^{-1} = \mathcal{I}_p - X^\top (\mathcal{I}_n + X X^\top)^{-1} X$ . This process successfully transfers the inverse operation of a  $p \times p$  matrix to a  $n \times n$  matrix, which greatly reduces the computational cost of the algorithm when  $p$  is much larger than  $n$ .

For the  $u$  and  $v$  subproblems, with the help of proximal point mapping, we can obtain

$$\begin{aligned} u^{k+1} &= \arg \min_{u \in \mathbb{R}^n} \left\{ \frac{\|u\|_2}{\sqrt{n}} - \langle z^k, u \rangle + \frac{\sigma}{2} \|X\beta^{k+1} - u - y\|^2 \right\} = \text{Prox}_{\frac{1}{\sigma\sqrt{n}} \|\cdot\|_2} (X\beta^{k+1} - y + \sigma^{-1} z^k). \\ v^{k+1} &= \arg \min_{v \in \mathbb{R}^p} \left\{ \frac{\lambda}{n} \|v\|_{G,\tau} - \langle w^k, v \rangle + \frac{\sigma}{2} \|\beta^{k+1} - v\|^2 \right\} = \text{Prox}_{\frac{\lambda}{\sigma n} \|\cdot\|_{G,\tau}} (\beta^{k+1} + \sigma^{-1} w^k). \end{aligned}$$

Denote  $r^{k+1} := X\beta^{k+1} - y + \sigma^{-1} z^k$ . From [1, Example 6.19], we have

$$\text{Prox}_{\frac{1}{\sigma\sqrt{n}} \|\cdot\|_2} (r^{k+1}) = \left( 1 - \frac{1}{\max\{\sigma\sqrt{n} \|r^{k+1}\|_2, 1\}} \right) r^{k+1}.$$

Let  $h^{k+1} := \beta^{k+1} + \sigma^{-1} w^k$ . To compute the proximal point of  $h^{k+1}$  associated with  $\frac{\lambda}{\sigma n} \|\cdot\|_{G,\tau}$ , we first give the following result:

**Lemma 3.1.** *If  $f(v) = \frac{\lambda}{\sigma n} \|v\|_{G,\tau}$ , we have*

$$\text{Prox}_f(x) = x - \Pi_{\mathcal{S}_\mathcal{O}}(x),$$

where  $\mathcal{O} := \{i \in [p] \mid \|x_{\mathcal{N}_i}\|_2 > \frac{\lambda\tau_i}{\sigma n}\}$ ,  $\mathcal{S}_\mathcal{O} := \{x \in \mathbb{R}^p \mid \|x_{\mathcal{N}_i}\|_2 \leq \frac{\lambda\tau_i}{\sigma n} \text{ for each } i \in \mathcal{O}\}$ .

*Proof.* See Appendix G. □

Then, it is easy to see that

$$\text{Prox}_{\frac{\lambda}{\sigma n} \|\cdot\|_{G,\tau}}(h^{k+1}) = h^{k+1} - \Pi_{S_{\mathcal{O}^{k+1}}}(h^{k+1}),$$

where  $\mathcal{O}^{k+1} := \{i \in [p] \mid \|h_{\mathcal{N}_i}^{k+1}\|_2 > \frac{\lambda \tau_i}{\sigma n}\}$ ,  $S_{\mathcal{O}^{k+1}} := \{x \in \mathbb{R}^p \mid \|x_{\mathcal{N}_i}\|_2 \leq \frac{\lambda \tau_i}{\sigma n} \text{ for each } i \in \mathcal{O}^{k+1}\}$ . The main problem we face is to solve the projection of  $h^{k+1}$  onto the convex set  $S_{\mathcal{O}^{k+1}}$ . Similar to [50], we also use different methods to calculate flexibly based on the number of elements in  $\mathcal{O}^{k+1}$ , denoted as  $|\mathcal{O}^{k+1}|$ . Specifically, when  $|\mathcal{O}^{k+1}| < p/10$ , we use the Bertsekas's projected Newton method [44] to calculate this projection from the dual perspective. However, when  $|\mathcal{O}^{k+1}| \geq p/10$ , we use the Parallel Dykstra-like proximal algorithm [10]. The details about these two algorithms are shown in the supplementary materials of [50].

Based on the above analysis, we see that each minimization subproblem has been effectively computed, and thus we can summarize the algorithm framework of ADMM for model (3.1).

### ADMM Algorithm

**Step 0:** Let  $\sigma > 0$ ,  $\tau \in (0, (1 + \sqrt{5})/2)$  be given parameters. Choose  $(u^0, v^0, z^0, w^0) \in \mathbb{R}^n \times \mathbb{R}^p \times \mathbb{R}^n \times \mathbb{R}^p$ . For  $k = 0, 1, \dots$ , perform the following steps iteratively:

**Step 1:** Given  $u^k, v^k, z^k$  and  $w^k$ , compute

$$\beta^{k+1} = \left(\mathcal{I}_p + X^\top X\right)^{-1} \left(v^k - \sigma^{-1} w^k + X^\top (u^k + y - \sigma^{-1} z^k)\right).$$

**Step 2:** Given  $\beta^{k+1}, z^k$  and  $w^k$ , compute

$$u^{k+1} = \text{Prox}_{\frac{1}{\sigma \sqrt{n}} \|\cdot\|_2}(X\beta^{k+1} - y + \sigma^{-1} z^k), \quad v^{k+1} = \text{Prox}_{\frac{\lambda}{\sigma n} \|\cdot\|_{G,\tau}}(\beta^{k+1} + \sigma^{-1} w^k).$$

**Step 3:** Given  $\beta^{k+1}, u^{k+1}, v^{k+1}, z^k$  and  $w^k$ , compute

$$z^{k+1} = z^k + \tau \sigma (X\beta^{k+1} - u^{k+1} - y), \quad w^{k+1} = w^k + \tau \sigma (\beta^{k+1} - v^{k+1}).$$

The non-interdependence of the  $u$  and  $v$  subproblems makes the above iterative framework equivalent to 2-block ADMM with guaranteed convergence. Specific convergence results are detailed in [15], and will not be further elaborated here.

## 4 Numerical experiments

To thoroughly evaluate the numerical performance of the proposed GSRE method, we compare it with several classic linear regression methods. Specifically, we compare it with well-established ridge regression (Ridge), lasso, adaptive lasso (Alasso) and elastic net (Enet), which do not utilize the structural information of the predictor graph. Their results are obtained by running their corresponding internal functions in MATLAB. Additionally, to highlight the advantages of the graph penalty in this paper, we compare GSRE with the traditional square-root lasso (SRL) in [3]. Furthermore, to demonstrate the advantages of the square-root loss in this paper, we compare GSRE with the graph sparse regression based on least squares loss, i.e., SRIG in [50].

## 4.1 Simulation data

In the simulation studies, the predictor graph is defined by the precision matrix of the predictors. In practice, the predictor graph is estimated by the graphical lasso method [18]. We also consider the performance of GSRE and SRIG with the true predictor graph, denoted as GSRE-o and SRIG-o, respectively. In the entire simulation experiment, we uniformly set  $p = 100$  and the true coefficient vector as  $\beta^* = (3, \dots, 3, 0, \dots, 0)^\top$  and  $s^* = 15$ . The simulated data consists of a training set, an independent validation set, and an independent test set. All models are fitted only on the training data. The validation set is used to choose the appropriate tuning parameter, and we use the BIC criterion to determine the optimal tuning parameter. The test set is used to evaluate the performance of different methods. We use the notation  $./././$  to denote the sample sizes in the training, validation and test sets, respectively. To highlight  $p > n$ , for each example, we consider three cases: (I) 20/20/400, (II) 40/40/400 and (III) 60/60/400. For each case, we repeat the simulation 50 times to observe the stability of the algorithms.

To ensure a comprehensive comparison, we consider three different predictor structures and four different types of noise. The methods for generating the predictors are as follows:

**Example 1:** The predictors are generated as:

$$\begin{aligned} X_j &= Z_1 + 0.4\epsilon_j^x, \quad Z_1 \sim N(0, 1), \quad 1 \leq j \leq 5; \\ X_j &= Z_2 + 0.4\epsilon_j^x, \quad Z_2 \sim N(0, 1), \quad 6 \leq j \leq 10; \\ X_j &= Z_3 + 0.4\epsilon_j^x, \quad Z_3 \sim N(0, 1), \quad 11 \leq j \leq 15; \\ X_j &\stackrel{i.i.d.}{\sim} N(0, 1), \quad 16 \leq j \leq 100, \\ \text{where } \epsilon_j^x &\stackrel{i.i.d.}{\sim} N(0, 1), \quad j = 1, 2, \dots, 15. \end{aligned}$$

**Example 2:** The predictors are generated as:

$$\begin{aligned} X_j &= Z_1 + 0.75\epsilon_j^x, \quad Z_1 \sim \text{Uniform}[-1, 1], \quad 1 \leq j \leq 5; \\ X_j &= Z_2 + 0.75\epsilon_j^x, \quad Z_2 \sim \text{Uniform}[-1, 1], \quad 6 \leq j \leq 10; \\ X_j &= Z_3 + 0.75\epsilon_j^x, \quad Z_3 \sim \text{Uniform}[-1, 1], \quad 11 \leq j \leq 15; \\ X_j &\stackrel{i.i.d.}{\sim} \text{Uniform}[-1, 1], \quad 16 \leq j \leq 100, \\ \text{where } \epsilon_j^x &\stackrel{i.i.d.}{\sim} \text{Uniform}[-1, 1], \quad j = 1, 2, \dots, 15. \end{aligned}$$

**Example 3:** The predictors  $(X_1, X_2, \dots, X_{100})^\top \sim N(0, \Sigma)$  with  $\Sigma_{ij} = 0.5^{|i-j|}$ .

Figure 1 illustrates the true predictor graphs of the three simulated examples. Since Examples 1 and 2 have the same correlation among predictors except for differences in their internal distributions, their predictor graph structures are identical. Since there are three groups of correlations among the first 15 predictors, the predictor graph contains three interconnected subgraphs. Because the remaining predictors are independent of each other, the predictor graph includes 85 isolated nodes. Due to their similarity, we have combined their experimental results. Assuming the precision matrix corresponding to the predictor graph is denoted by  $\Omega = (\omega_{ij})_{i,j=1,2,\dots,p}$ , the generation method for Example 3 leads to  $\omega_{ii} = 1.333$ ,  $\omega_{ij} = -0.667$  if  $|i - j| = 1$  and  $\omega_{ij} = 0$  if  $|i - j| > 1$ . This indicates that predictors are only correlated with variables in their neighborhood, resulting in a banded structure for the predictor graph.

To account for the diversity of noise types, we will describe four different types of noise:

- Normal distribution:  $\epsilon \sim N(0, 5^2)$ .
- T-distribution:  $\epsilon \sim t(10)/2\sqrt{5}$ .

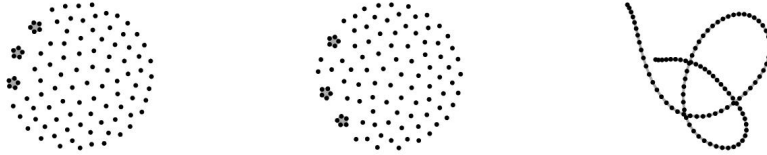


Figure 1: True predictor graphs of three simulated examples.

- Laplace distribution:  $\epsilon \sim \text{Laplace}(0, 5/\sqrt{2})$ .
- Uniform distribution:  $\epsilon \sim \text{Uniform}[-5\sqrt{3}, 5\sqrt{3}]$ .

Here, we consider normal distribution with high noise levels, t-distribution with heavier tails, laplace distribution with high kurtosis, and uniform distribution presenting a scenario with constant probability. These all create challenging statistical environments. To evaluate the performances of different methods, we use the following measures:

- $L_2$  distance =  $\|\hat{\beta} - \beta^*\|_2$ ;
- Relative prediction error (RPE) =  $\frac{1}{\sigma^2 N_{test}} (\hat{\beta} - \beta^*)^\top X_{test}^\top X_{test} (\hat{\beta} - \beta^*)$ , where  $X_{test}$  is the test samples and  $N_{test}$  is the number of test samples;
- False positive rate (FPR) and false negative rate (FNR).

Tables 1-4 show the performance of each method for Examples 1 and 2 under four different types of noise. The numbers in parentheses represent the corresponding standard deviations, which are used to measure the stability of these methods. A review of the results in the tables shows that the patterns presented in the four tables are similar. Specifically, among the five methods that do not utilize the predictor graph structure information, Enet achieves better estimation results. Alasso performs better in both RPE and FPR. Although Ridge has the smallest FNR, its FPR is nearly 1. This phenomenon indicates that nearly all zero elements are estimated as non-zero elements. In cases (I) and (II), where  $p \gg n$ , the proposed GSRE method generally performs best in estimation, prediction and model selection for Example 1 and Example 2. Although in case (I), the FNR of GSRE is slightly higher than that of SRIG for Example 2, it is noteworthy that our FPR is significantly lower than that of SRIG. This observation clearly indicates that our method also outperforms SRIG in model selection. For case (III), where the sample size is slightly larger, GSRE remains optimal in model estimation and prediction, but is slightly

inferior to SRIG in model selection. Additionally, we find that for Example 1 and Example 2, the results using the estimated predictor graph and the true predictor graph are almost identical, and sometimes the performance with the true predictor graph is slightly worse than that with the estimated predictor graph. This discrepancy may be due to inherent precision issues in MATLAB when computing the inverse of the covariance matrix corresponding to the true predictor graph.

Tables 5-8 display the performance of each method for Example 3 under four different types of noise. Similarly, as the sample size increases, the numerical performance of each algorithm improves. Ridge regression shows a low FNR but a high FPR, which indicate a tendency towards overfitting. Lasso and Alasso methods generally have lower values of FPR, but they have higher values for  $L_2$  distance and FNR. In all four challenging environments, the GSRE method consistently outperforms other methods in model estimation and prediction, which shows its robust performance. By balancing the values of FPR and FNR, it is clear that our method also performs very well in model selection for Example 3.

In summary, the simulation results indicate that methods incorporating graphical structure among predictors outperform popular penalization methods. In various noise environments, the proposed GSRE method, which combines square-root estimation with graph penalty, demonstrates superior performance in estimation, prediction and model selection. This result highlights the general applicability and reliability of the GSRE method in statistical modeling.

## 4.2 Real data

In this part, we further evaluate the numerical performance of the GSRE method by two real data sets.

The first set is the bodyfat2 data, which originates from the bodyfat data in the LIBSVM database. This data is suitable for large-scale regression problems and can be available at <https://www.csie.ntu.edu.tw/~cjlin/libsvmtools/datasets>. For this study, we first preprocess the data by removing zero columns. Additionally, we use the method of [22] to expand the data by applying polynomial basis functions to the original features. The final digit 2 in bodyfat2 indicates that we use second-order polynomials to generate the basis functions. After expansion, we obtain the bodyfat2 data with a sample size of 252 and a dimensionality of 120. To satisfy the high-dimensional assumption, i.e.,  $p > n$ , we randomly select 100 samples. Therefore the size of the data set we employ is  $100 \times 120$ .

The second set is the miRNA data, which is a small noncoding RNAs that play a crucial role in various biological processes such as development, cellular differentiation, cell cycle regulation and programmed cell death. Recent studies have shown a strong association between miRNA and cancer [19, 21, 25]. Here, we use the miRNA expression data for thymic cancer, which can be downloaded from R package. This data is sourced from thymoma tissue samples in the Cancer Genome Atlas database. This data set provides miRNA expression values for 113 patients across 1,881 miRNAs. After removing duplicate features and filtering out low-expression genes, we obtained expression values for 136 miRNAs. Consequently, the data size is  $113 \times 136$ , which satisfies the high-dimensional assumption of  $p > n$ . We also consider survival time as the response variable  $y$ .

Before inputting the preprocessed data into the algorithm for iteration, we perform normalization on the data sets. We then use the graphical lasso [18] to estimate the graphical structure of the predictors, as detailed in Figure 2. It is evident that there is a high degree of correlation among the predictors in both data sets.

In the specific experiments, we use ten-fold cross-validation to evaluate different methods. Here, we randomly select nine folds of data as the training set and use the remaining data as the test set. All models are fitted on the training set and evaluated on the test data. To select the tuning parameters for different methods, we use five-fold cross-validation on the training set. We repeat the experiment

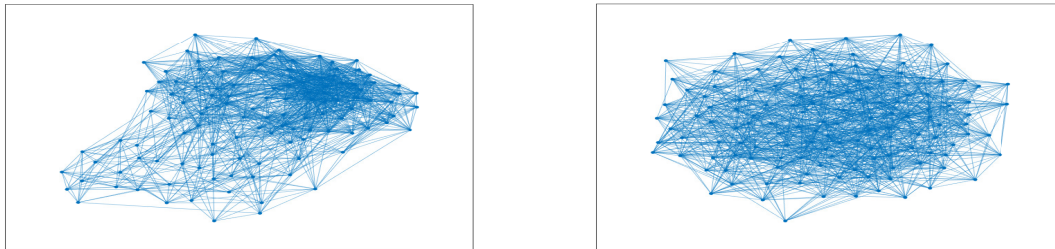


Figure 2: Estimated graphs of real data. Left:bodyfat2. Right:miRNA.

10 times to avoid bias introduced by random partitioning. Here, we uniformly use mean squared error (MSE) to measure prediction accuracy.

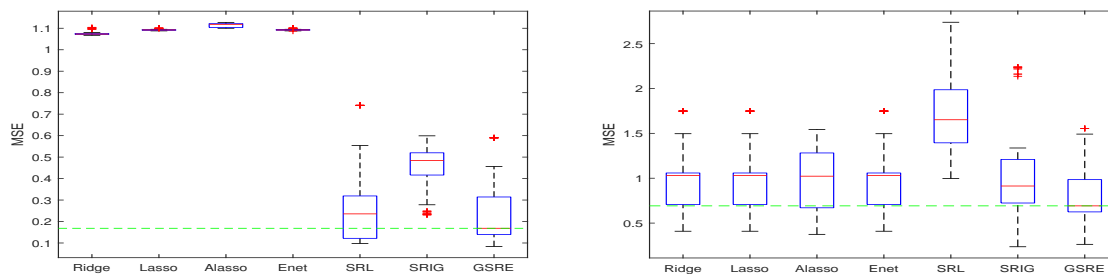


Figure 3: Comparison of MSE for various methods on real data. Left:bodyfat2. Right:miRNA.

Figure 3 shows box plots of MSE from 10 repeated experiments for different methods on two real data sets. Figure 3 (a) illustrates the performance of various methods on the bodyfa2 data. The results indicate that GSRE significantly outperforms Ridge, Lasso, Alasso, Enet and SRIG in terms of MSE scores. Although the box sizes of GSRE and SRL are similar, GSRE’s median is noticeably lower than that of SRL. Figure 3 (b) presents the numerical performance of different methods on the miRNA data. This figure clearly shows that GSRE’s median is significantly lower than that of other methods. These results indicate that the GSRE method has superior numerical performance compared to other methods and is an ideal choice for achieving accurate predictions.

## 5 Conclusion

In this paper, we addresses the high-dimensional sparse linear regression problem by proposing a graph-based square-root estimation (GSRE) method, which integrates square-root loss and node-wise graph penalty. This paper highlights the broad applicability of the proposed method by analyzing its equivalence with several classical square-root estimation models. A notable feature of the theoretical analysis is that the tuning parameter no longer depends on the unknown standard deviation of the error terms. Additionally, we establish theoretical results on finite sample bounds and model selection consistency. In terms of computation, we use the fast and efficient alternating direction method of multipliers. Extensive simulation and real tests demonstrate that the proposed GSRE method is a competitive tool for estimation, prediction and model selection. Future work will consider extending this approach to more general loss functions, such as  $\ell_p$  ( $p \geq 1$ ) loss [45, 47, 48, 54], which will facilitate the

handling of a broader range of noise types in high-dimensional settings.

## Acknowledgements

The authors report there are no competing interests to declare. All authors read and approved the final manuscript. The work of Peili Li is supported by the National Natural Science Foundation of China (Grant No. 12301420). The work of Yunhai Xiao is supported by the National Natural Science Foundation of China (Grant No. 12471307 and 12271217), the National Natural Science Foundation of Henan Province (Grant No. 232300421018). The work of Zhou Yu is supported by the National Key R&D Program of China (Grant No. 2023YFA1008700 and 2023YFA1008703), the National Natural Science Foundation of China (Grant No. 12371289), the Basic Research Project of Shanghai Science and Technology Commission (Grant No. 22JC1400800) and the Shanghai Pilot Program for Basic Research (Grant No. TQ20220105).

## A Proof of Lemma 2.1

**Proof.** Define  $\mathcal{L}(\beta) = \frac{\|y - X\beta\|_2}{\sqrt{n}}$  and denote  $\partial_{\mathcal{N}_i} \mathcal{L}(\beta) \in \mathbb{R}^{d_i}$  as the partial subdifferential sets of  $\mathcal{L}(\beta)$  with respect to the predictors in  $\mathcal{N}_i$ . Then, with the help of subdifferential of the  $\ell_2$ -norm in [1, Example 3.34], we have  $\frac{X_{\mathcal{N}_i}^\top (X\beta - y)}{\sqrt{n}\|y - X\beta\|_2} \in \partial_{\mathcal{N}_i} \mathcal{L}(\beta)$ . Therefore, the conclusions of Lemma 2.1 can be derived immediately from [34, Lemma 11].

## B Proof of Lemma 2.2

**Proof.**

- (a) If the predictor graph has no edge, then  $\mathcal{N}_i = \{i\}$  for each  $i \in [p]$ , and

$$\|\beta\|_{G,\tau} = \min_{\sum_{i=1}^p V^{(i)} = \beta, \text{supp}(V^{(i)}) \subseteq \mathcal{N}_i} \sum_{i=1}^p \tau_i \|V^{(i)}\|_2 = \sum_{i=1}^p \tau_i |\beta_i|.$$

Therefore, at this time, problem (1.4) is the same as (2.1). When  $\tau_i \equiv 1$  for each  $i$ , we have  $\|\beta\|_{G,\tau} = \sum_{i=1}^p |\beta_i| = \|\beta\|_1$ . Therefore, (2.1) is the classic square-root lasso.

- (b) From the hypothesis, for  $1 \leq j \leq J$  and  $q_{j-1} + 1 \leq l \leq q_{j-1} + q_j$ , we have  $\mathcal{N}_l = \{q_{j-1} + 1, \dots, q_{j-1} + q_j\}$ . In addition, for each  $j$ , we have  $\beta^{(j)} = \sum_{l=q_{j-1}+1}^{q_{j-1}+q_j} V_{\mathcal{N}_l}^{(l)}$ . Then,

$$\|\beta\|_{G,\tau} = \sum_{j=1}^J \|\beta^{(j)}\|_{G,\tau} = \sum_{j=1}^J \min_{\sum_{l=q_{j-1}+1}^{q_{j-1}+q_j} V_{\mathcal{N}_l}^{(l)} = \beta^{(j)}} \sum_{l=q_{j-1}+1}^{q_{j-1}+q_j} \tau_l \|V_{\mathcal{N}_l}^{(l)}\|_2.$$

Combining the definition of  $\tilde{\tau}_j$  and the inequality  $\|\sum_{i=1}^n a_i\|_2 \leq \sum_{i=1}^n \|a_i\|_2$ , we have

$$\|\beta\|_{G,\tau} = \sum_{j=1}^J \tilde{\tau}_j \|\beta^{(j)}\|_2.$$

Therefore, at this time, problem (1.4) is equivalent to the problem (2.2).

- (c) If the predictor graph is a complete graph, by the proof of (b) with  $J = 1$ , we have the problem (1.4) is equivalent to

$$\min_{\beta \in \mathbb{R}^p} \left\{ \frac{\|y - X\beta\|_2}{\sqrt{n}} + \frac{\lambda \tilde{\tau}}{n} \|\beta\|_2 \right\}. \quad (\text{A.1})$$

Denote  $\mathcal{L}(\beta) = \frac{\|y - X\beta\|_2}{\sqrt{n}}$ , then we have the nonzero solution  $\hat{\beta}_\lambda$  of (A.1) satisfies  $\mathbf{0}_p \in \partial \mathcal{L}(\hat{\beta}_\lambda) + \frac{\lambda \tilde{\tau}}{n} \frac{\hat{\beta}_\lambda}{\|\hat{\beta}_\lambda\|_2}$ . Thus,  $\hat{\beta}_\lambda$  is also the solution of (2.3) with  $\tilde{\lambda} = \frac{\lambda \tilde{\tau}}{2\|\hat{\beta}_\lambda\|_2}$ . In addition, if  $\hat{\beta}_{\tilde{\lambda}}$  is the solution of (2.3) with tuning parameter  $\tilde{\lambda}$ , we have  $\mathbf{0}_p \in \partial \mathcal{L}(\hat{\beta}_{\tilde{\lambda}}) + \frac{2\tilde{\lambda}}{n} \hat{\beta}_{\tilde{\lambda}}$ . Then  $\hat{\beta}_{\tilde{\lambda}}$  is also the solution of (A.1) with  $\lambda = \frac{2\tilde{\lambda}\|\hat{\beta}_{\tilde{\lambda}}\|_2}{\tilde{\tau}}$ . Therefore, at this time, problem (1.4) has the same nonzero solutions as the problem (2.3).

## C Proof of Lemma 2.3

**Proof.** Denote  $\lambda_0 = \frac{n\sqrt{2\zeta d_{max}}}{\tau_{min}\sqrt{n-d_{max}}}\left(1 + \sqrt{\frac{2\log(2p/\alpha)}{d_{min}}}\right)$ , then we have  $\frac{\lambda}{\bar{r}} \geq \lambda_0$ . Therefore, to achieve the proof of this lemma, we only need to prove that  $\mathbb{P}(V \geq \lambda_0) \leq \alpha$ . Then we have

$$\begin{aligned} \mathbb{P}(V \geq \lambda_0) &= \mathbb{P}\left(\max_{1 \leq i \leq p} \frac{\sqrt{n}\|X_{\mathcal{N}_i}^\top \epsilon\|_2}{\tau_i \|\epsilon\|_2} \geq \lambda_0\right) = \mathbb{P}\left(\max_{1 \leq i \leq p} \frac{\|X_{\mathcal{N}_i}^\top \epsilon\|_2^2}{n\tau_i^2 \|\epsilon\|_2^2} \geq \frac{\lambda_0^2}{n^2}\right) \\ &= \mathbb{P}\left(\max_{1 \leq i \leq p} \epsilon^\top \left(\frac{X_{\mathcal{N}_i} X_{\mathcal{N}_i}^\top}{n} - \frac{\lambda_0^2 \tau_i^2}{n^2} I\right) \epsilon \geq 0\right) \leq \sum_{i=1}^p \mathbb{P}\left(\epsilon^\top \left(\frac{X_{\mathcal{N}_i} X_{\mathcal{N}_i}^\top}{n} - \frac{\lambda_0^2 \tau_i^2}{n^2} I\right) \epsilon \geq 0\right). \end{aligned}$$

Let  $U_i^\top D_i U_i$  be a spectral decomposition of  $\frac{X_{\mathcal{N}_i} X_{\mathcal{N}_i}^\top}{n}$  such that  $U_i$  is orthogonal and  $D_i$  is diagonal with diagonal entries  $\xi_1^i \geq \dots \geq \xi_{d_i}^i \geq \xi_{d_i+1}^i = \dots = \xi_n^i = 0$ . With the notation  $\zeta_i = \|X_{\mathcal{N}_i}\|^2/n$ , we have  $\zeta_i = \xi_1^i$ . It follows that

$$\begin{aligned} \epsilon^\top \left(\frac{X_{\mathcal{N}_i} X_{\mathcal{N}_i}^\top}{n} - \frac{\lambda_0^2 \tau_i^2}{n^2} I\right) \epsilon &= \epsilon^\top \left(U_i^\top D_i U_i - \frac{\lambda_0^2 \tau_i^2}{n^2} I\right) \epsilon \\ &= (U_i \epsilon)^\top \left(D_i - \frac{\lambda_0^2 \tau_i^2}{n^2} I\right) U_i \epsilon \leq \|\epsilon_1\|_2^2 \left(\zeta_i - \frac{\lambda_0^2 \tau_i^2}{n^2}\right)_+ - \|\epsilon_2\|_2^2 \frac{\lambda_0^2 \tau_i^2}{n^2}. \end{aligned}$$

where  $\epsilon_1$  and  $\epsilon_2$  are independent with  $\epsilon_1 \sim \mathcal{N}(0, I_{d_i})$  and  $\epsilon_2 \sim \mathcal{N}(0, I_{(n-d_i)})$ . Thus, for any fixed  $\gamma \in (0, 1)$ , we have

$$\begin{aligned} \mathbb{P}(V \geq \lambda_0) &\leq \sum_{i=1}^p \mathbb{P}\left(\frac{n^2 \|\epsilon_1\|_2^2}{\lambda_0^2 \tau_i^2} \left(\zeta_i - \frac{\lambda_0^2 \tau_i^2}{n^2}\right)_+ \geq \|\epsilon_2\|_2^2\right) \\ &\leq \sum_{i=1}^p \mathbb{P}\left(\frac{\|\epsilon_1\|_2^2}{\tau_i^2} \left(\frac{n^2 \zeta_i}{\lambda_0^2} - \tau_i^2\right)_+ \frac{1}{n-d_i} \geq 1-\gamma\right) + \sum_{i=1}^p \mathbb{P}\left(\frac{\|\epsilon_2\|_2^2}{n-d_i} \leq 1-\gamma\right). \end{aligned} \quad (\text{A.2})$$

If  $\zeta_i \leq \frac{\lambda_0^2 \tau_i^2}{n^2}$ , then the first sum in the inequality above is trivially equal to zero. At this point, it suffices to show that the second sum is controlled by  $\alpha$ . Thus, we will subsequently examine that both sums in (A.2) are controlled by  $\frac{\alpha}{2}$  under the assumption that  $\zeta_i > \frac{\lambda_0^2 \tau_i^2}{n^2}$ . From [26, Lemma 1],  $\mathbb{P}(X - d \geq dt) \leq \exp(-\frac{d}{4}(\sqrt{1+2t}-1)^2)$  and  $\mathbb{P}(X \leq d - dt) \leq \exp(-\frac{d}{4}t^2)$ , for  $X \sim \mathcal{X}^2(d)$ . Then, for each  $i$  in the first sum of (A.2), we can obtain:

$$\begin{aligned} \mathbb{P}\left(\frac{\|\epsilon_1\|_2^2}{\tau_i^2} \left(\frac{n^2 \zeta_i}{\lambda_0^2} - \tau_i^2\right) \frac{1}{n-d_i} \geq 1-\gamma\right) &= \mathbb{P}\left(\frac{\|\epsilon_1\|_2^2 - d_i}{\tau_i^2} \geq \frac{(1-\gamma)(n-d_i)}{\frac{n^2 \zeta_i}{\lambda_0^2} - \tau_i^2} - \frac{d_i}{\tau_i^2}\right) \\ &= \mathbb{P}\left(\|\epsilon_1\|_2^2 - d_i \geq d_i \left(\frac{\tau_i^2(1-\gamma)(n-d_i)}{d_i(\frac{n^2 \zeta_i}{\lambda_0^2} - \tau_i^2)} - 1\right)\right) \leq \exp\left(-\frac{d_i}{4} \left(\sqrt{\frac{2\tau_i^2(1-\gamma)(n-d_i)}{d_i(\frac{n^2 \zeta_i}{\lambda_0^2} - \tau_i^2)} - 1 - 1}\right)^2\right) \\ &\leq \exp\left(-\frac{d_{min}}{4} \left(\sqrt{\frac{2\tau_{min}^2(1-\gamma)(n-d_{max})}{d_{max}(\frac{n^2 \zeta}{\lambda_0^2} - \tau_{min}^2)} - 1 - 1}\right)^2\right). \end{aligned}$$

To bound the last term in (A.2), for each  $i$ , we can obtain:

$$\mathbb{P}\left(\frac{\|\epsilon_2\|_2^2}{n-d_i} \leq 1-\gamma\right) \leq \exp\left(-\frac{(n-d_i)\gamma^2}{4}\right) \leq \exp\left(-\frac{(n-d_{max})\gamma^2}{4}\right).$$

Hence,

$$\begin{aligned} \mathbb{P}(V \geq \lambda_0) &\leq p \cdot \exp\left(-\frac{d_{\min}}{4} \left(\sqrt{\frac{2\tau_{\min}^2(1-\gamma)(n-d_{\max})}{d_{\max}(\frac{n^2\xi}{\lambda_0^2} - \tau_{\min}^2)}} - 1 - 1\right)^2\right) \\ &\quad + p \cdot \exp\left(-\frac{(n-d_{\max})\gamma^2}{4}\right). \end{aligned}$$

For  $\gamma = 2\sqrt{\frac{\log(2p/\alpha)}{n-d_{\max}}}$ , the last term of the above expression is bounded by  $\alpha/2$ . In addition, combining the values of  $\gamma$  and  $\lambda_0$ , the first term in the above equation is also controlled by  $\alpha/2$ . Therefore, we have  $\mathbb{P}(V \geq \lambda_0) \leq \alpha$ .

## D Proof of Theorem 2.1

The proof of Theorem 2.1 requires the following two lemmas. To avoid repetition, only the contents of the relevant lemmas are presented here without detailed proofs. Interested readers can refer to relevant literature for more information.

**Lemma 4.1.** [50, Lemma 2 in supplementary materials] *For any predictor graph  $G$  and positive weights  $\tau_1, \tau_2, \dots, \tau_p$ , suppose  $V^{(1)}, V^{(2)}, \dots, V^{(p)}$  is an optimal decomposition of  $\beta \in \mathbb{R}^p$ , then for any  $S \subset [p]$ ,  $\{V^{(i)} : i \in S\}$  is also an optimal decomposition of  $\sum_{i \in S} V^{(i)}$ .*

**Lemma 4.2.** [12, Lemma 7.6] *With probability at least  $1 - (1 + e^2)e^{-n/24}$ , we have*

$$\frac{\sigma}{\sqrt{2}} \leq \frac{\|\sigma\epsilon\|_2}{\sqrt{n}} \leq 2\sigma.$$

Based on the above two lemmas, we now can give the detailed proof of Theorem 2.1.

**Proof.** Because  $\hat{\beta}$  is an optimal solution of problem (1.4), then we have

$$\frac{\|y - X\hat{\beta}\|_2}{\sqrt{n}} - \frac{\|y - X\beta^*\|_2}{\sqrt{n}} \leq \frac{\lambda}{n} \left( \|\beta^*\|_{G,\tau} - \|\hat{\beta}\|_{G,\tau} \right). \quad (\text{A.3})$$

Let  $\hat{\delta} = \hat{\beta} - \beta^*$ ,  $(S^{(1)}, S^{(2)}, \dots, S^{(p)})$  as an arbitrary optimal decomposition of  $\beta^*$  and  $(T^{(1)}, T^{(2)}, \dots, T^{(p)})$  as an arbitrary optimal decomposition of  $\hat{\delta}$ . Then, by the Assumption 2.2, we get

$$\begin{aligned} \|\hat{\beta}\|_{G,\tau} &= \|\hat{\beta} - \beta^* + \beta^*\|_{G,\tau} = \left\| \sum_{i \in \mathcal{I}_*} T^{(i)} + \sum_{i \in \mathcal{I}_*^c} T^{(i)} + \sum_{i \in \mathcal{I}_*} S^{(i)} \right\|_{G,\tau} \\ &\geq \left\| \sum_{i \in \mathcal{I}_*^c} T^{(i)} + \sum_{i \in \mathcal{I}_*} S^{(i)} \right\|_{G,\tau} - \left\| \sum_{i \in \mathcal{I}_*} T^{(i)} \right\|_{G,\tau} \\ &= \left\| \sum_{i \in \mathcal{I}_*^c} T^{(i)} \right\|_{G,\tau} + \left\| \sum_{i \in \mathcal{I}_*} S^{(i)} \right\|_{G,\tau} - \left\| \sum_{i \in \mathcal{I}_*} T^{(i)} \right\|_{G,\tau}. \end{aligned}$$

Next, by Lemma 4.1, we have

$$\begin{aligned} \|\beta^*\|_{G,\tau} - \|\hat{\beta}\|_{G,\tau} &\leq \left\| \sum_{i \in \mathcal{I}_*} S^{(i)} \right\|_{G,\tau} - \left\| \sum_{i \in \mathcal{I}_*^c} T^{(i)} \right\|_{G,\tau} - \left\| \sum_{i \in \mathcal{I}_*} S^{(i)} \right\|_{G,\tau} + \left\| \sum_{i \in \mathcal{I}_*} T^{(i)} \right\|_{G,\tau} \\ &= \left\| \sum_{i \in \mathcal{I}_*} T^{(i)} \right\|_{G,\tau} - \left\| \sum_{i \in \mathcal{I}_*^c} T^{(i)} \right\|_{G,\tau} = \sum_{i \in \mathcal{I}_*} \tau_i \|T^{(i)}\|_2 - \sum_{i \in \mathcal{I}_*^c} \tau_i \|T^{(i)}\|_2. \end{aligned}$$

Combining inequality (A.3) and  $\lambda > 0$ , we can obtain

$$\frac{\|y - X\hat{\beta}\|_2}{\sqrt{n}} - \frac{\|y - X\beta^*\|_2}{\sqrt{n}} \leq \frac{\lambda}{n} \sum_{i \in \mathcal{I}_*} \tau_i \|T^{(i)}\|_2 - \frac{\lambda}{n} \sum_{i \in \mathcal{I}_c^c} \tau_i \|T^{(i)}\|_2. \quad (\text{A.4})$$

In addition, from the convexity of the norm  $\|y - X\beta\|_2$ , we have

$$\frac{\|y - X\hat{\beta}\|_2}{\sqrt{n}} - \frac{\|y - X\beta^*\|_2}{\sqrt{n}} \geq \left\langle \frac{X^\top(X\beta^* - y)}{\sqrt{n}\|y - X\beta^*\|_2}, \hat{\delta} \right\rangle = \left\langle -\frac{X^\top \epsilon}{\sqrt{n}\|\epsilon\|_2}, \hat{\delta} \right\rangle \geq -\frac{|\epsilon^\top X \hat{\delta}|}{\sqrt{n}\|\epsilon\|_2}. \quad (\text{A.5})$$

Next, by using the Cauchy-Schwarz's inequality and recalling the definition of the error term  $V$ , we can see that

$$\begin{aligned} |\epsilon^\top X \hat{\delta}| &= \left| \epsilon^\top \left( \sum_{i=1}^p X_{\mathcal{N}_i} T_{\mathcal{N}_i}^{(i)} \right) \right| = \left| \epsilon^\top \left( \sum_{i=1}^p X_{\mathcal{N}_i} \cdot \frac{\sqrt{n}}{\tau_i \|\epsilon\|_2} \cdot \frac{\tau_i \|\epsilon\|_2}{\sqrt{n}} \cdot T_{\mathcal{N}_i}^{(i)} \right) \right| \\ &\leq \sum_{i=1}^p \frac{\sqrt{n} \|X_{\mathcal{N}_i}^\top \epsilon\|_2}{\tau_i \|\epsilon\|_2} \cdot \frac{\tau_i \|\epsilon\|_2}{\sqrt{n}} \|T_{\mathcal{N}_i}^{(i)}\|_2 \leq V \frac{\|\epsilon\|_2}{\sqrt{n}} \sum_{i=1}^p \tau_i \|T_{\mathcal{N}_i}^{(i)}\|_2 \leq V \frac{\|\epsilon\|_2}{\sqrt{n}} \sum_{i=1}^p \tau_i \|T^{(i)}\|_2. \end{aligned} \quad (\text{A.6})$$

Then, from (A.5), we have  $\frac{\|y - X\hat{\beta}\|_2}{\sqrt{n}} - \frac{\|y - X\beta^*\|_2}{\sqrt{n}} \geq -\frac{V}{n} \sum_{i=1}^p \tau_i \|T^{(i)}\|_2$ . Then by the definition of set  $\mathcal{A}$ , we can obtain  $\frac{\|y - X\hat{\beta}\|_2}{\sqrt{n}} - \frac{\|y - X\beta^*\|_2}{\sqrt{n}} \geq -\frac{\lambda}{n\bar{r}} \sum_{i=1}^p \tau_i \|T^{(i)}\|_2$ . Further, from (A.4), we get

$$-\frac{\lambda}{n\bar{r}} \sum_{i=1}^p \tau_i \|T^{(i)}\|_2 \leq \frac{\lambda}{n} \sum_{i \in \mathcal{I}_*} \tau_i \|T^{(i)}\|_2 - \frac{\lambda}{n} \sum_{i \in \mathcal{I}_c^c} \tau_i \|T^{(i)}\|_2.$$

After simple algebraic calculations, we can find  $\sum_{i \in \mathcal{I}_*} \tau_i \|T^{(i)}\|_2 \leq r \sum_{i \in \mathcal{I}_*} \tau_i \|T^{(i)}\|_2$ , which implies  $(T^{(1)}, T^{(2)}, \dots, T^{(p)}) \in \mathcal{T}_{G,\tau}(\hat{\delta}, \mathcal{I}_*)$ .

In addition, from (A.4), we have  $\frac{\|y - X\hat{\beta}\|_2}{\sqrt{n}} - \frac{\|y - X\beta^*\|_2}{\sqrt{n}} \leq \frac{\lambda}{n} \sum_{i \in \mathcal{I}_*} \tau_i \|T^{(i)}\|_2$ . Then we can use Assumption 2.3 to obtain

$$\sum_{i \in \mathcal{I}_*} \tau_i \|T^{(i)}\|_2 \leq \frac{\sqrt{s^*} \|X \hat{\delta}\|_2}{\sqrt{n} \kappa}. \quad (\text{A.7})$$

Then,

$$\frac{\|y - X\hat{\beta}\|_2}{\sqrt{n}} - \frac{\|y - X\beta^*\|_2}{\sqrt{n}} \leq \frac{\lambda \sqrt{s^*} \|X \hat{\delta}\|_2}{n^{\frac{3}{2}} \kappa}. \quad (\text{A.8})$$

Next, we can write

$$\begin{aligned} \frac{\|y - X\hat{\beta}\|_2^2}{n} - \frac{\|y - X\beta^*\|_2^2}{n} &= \frac{\|y - X\beta^* + X\beta^* - X\hat{\beta}\|_2^2}{n} - \frac{\sigma^2 \|\epsilon\|_2^2}{n} \\ &= \frac{\|X\hat{\delta} - \sigma\epsilon\|_2^2}{n} - \frac{\sigma^2 \|\epsilon\|_2^2}{n} = \frac{\|X\hat{\delta}\|_2^2}{n} - \frac{2\sigma\epsilon^\top X\hat{\delta}}{n}. \end{aligned}$$

Then, we have

$$\frac{\|X\hat{\delta}\|_2^2}{n} = \frac{\|y - X\hat{\beta}\|_2^2}{n} - \frac{\|y - X\beta^*\|_2^2}{n} + \frac{2\sigma\epsilon^\top X\hat{\delta}}{n} \leq \frac{\|y - X\hat{\beta}\|_2^2}{n} - \frac{\|y - X\beta^*\|_2^2}{n} + \frac{2\sigma|\epsilon^\top X\hat{\delta}|}{n}. \quad (\text{A.9})$$

Firstly, for the first two items on the right side of the above formula, we have

$$\begin{aligned} \frac{\|y - X\hat{\beta}\|_2^2}{n} - \frac{\|y - X\beta^*\|_2^2}{n} &= \left( \frac{\|y - X\hat{\beta}\|_2}{\sqrt{n}} - \frac{\|y - X\beta^*\|_2}{\sqrt{n}} \right) \times \left( \frac{\|y - X\hat{\beta}\|_2}{\sqrt{n}} + \frac{\|y - X\beta^*\|_2}{\sqrt{n}} \right) \\ &= \left( \frac{\|y - X\hat{\beta}\|_2}{\sqrt{n}} - \frac{\|y - X\beta^*\|_2}{\sqrt{n}} \right) \times \left( \frac{\|y - X\hat{\beta}\|_2}{\sqrt{n}} - \frac{\|y - X\beta^*\|_2}{\sqrt{n}} + \frac{2\|y - X\beta^*\|_2}{\sqrt{n}} \right) \\ &\leq \frac{\lambda\sqrt{s^*}\|X\hat{\delta}\|_2}{n^{\frac{3}{2}}\kappa} \left( \frac{\lambda\sqrt{s^*}\|X\hat{\delta}\|_2}{n^{\frac{3}{2}}\kappa} + \frac{2\sigma\|\epsilon\|_2}{\sqrt{n}} \right) = \frac{\lambda^2 s^* \|X\hat{\delta}\|_2^2}{n^3 \kappa^2} + \frac{2\sigma\lambda\sqrt{s^*}\|X\hat{\delta}\|_2\|\epsilon\|_2}{n^2 \kappa}. \end{aligned}$$

Additionally, for the third item on the right side of (A.9), we can use (A.6), (A.7) and  $V \leq \frac{\lambda}{\bar{r}}$  to deduce that

$$\begin{aligned} \frac{2\sigma|\epsilon^\top X\hat{\delta}|}{n} &\leq \frac{2\sigma V\|\epsilon\|_2}{n^{\frac{3}{2}}} \sum_{i=1}^p \tau_i \|T^{(i)}\|_2 \leq \frac{2\sigma V(1+r)\|\epsilon\|_2}{n^{\frac{3}{2}}} \sum_{i \in \mathcal{I}_*} \tau_i \|T^{(i)}\|_2 \\ &\leq \frac{2\sigma V(1+r)\|\epsilon\|_2 \sqrt{s^*}\|X\hat{\delta}\|_2}{n^2 \kappa} \leq \frac{2\sigma\lambda(1+r)\sqrt{s^*}\|X\hat{\delta}\|_2\|\epsilon\|_2}{\bar{r}n^2 \kappa}. \end{aligned}$$

Then, we can get

$$\begin{aligned} \frac{\|X\hat{\delta}\|_2^2}{n} &\leq \frac{\lambda^2 s^* \|X\hat{\delta}\|_2^2}{n^3 \kappa^2} + \frac{2\sigma\lambda\sqrt{s^*}\|X\hat{\delta}\|_2\|\epsilon\|_2}{n^2 \kappa} + \frac{2\sigma\lambda(1+r)\sqrt{s^*}\|X\hat{\delta}\|_2\|\epsilon\|_2}{\bar{r}n^2 \kappa} \\ &= \frac{\lambda^2 s^* \|X\hat{\delta}\|_2^2}{n^3 \kappa^2} + \frac{2\sigma\lambda\sqrt{s^*}\|X\hat{\delta}\|_2\|\epsilon\|_2}{n^2 \kappa} \left( 1 + \frac{1+r}{\bar{r}} \right) \\ &= \frac{\lambda^2 s^* \|X\hat{\delta}\|_2^2}{n^3 \kappa^2} + \frac{2\sigma r\lambda\sqrt{s^*}\|X\hat{\delta}\|_2\|\epsilon\|_2}{n^2 \kappa}. \end{aligned}$$

Consequently,

$$\left( 1 - \frac{\lambda^2 s^*}{n^2 \kappa^2} \right) \frac{\|X\hat{\delta}\|_2^2}{n} \leq \frac{2\sigma r\lambda\sqrt{s^*}\|X\hat{\delta}\|_2\|\epsilon\|_2}{n^2 \kappa}.$$

From Assumption 2.4, i.e.,  $s^* < \frac{n^2 \kappa^2}{\lambda^2}$ , we have

$$\frac{\|X\hat{\delta}\|_2^2}{n} \leq C \frac{\sigma\lambda\sqrt{s^*}\|X\hat{\delta}\|_2\|\epsilon\|_2}{n^2 \kappa},$$

where  $C := \frac{2r}{1 - \frac{\lambda^2 s^*}{n^2 \kappa^2}} > 0$ . Then, by Lemma 4.2, we further obtain that with probability at least  $1 - (1 + e^2)e^{-n/24}$ ,

$$\frac{\|X(\hat{\beta} - \beta^*)\|_2}{\sqrt{n}} \leq C \frac{\sigma\lambda\sqrt{s^*}\|\epsilon\|_2}{n^{\frac{3}{2}}\kappa} \leq 2C \frac{\sigma\lambda\sqrt{s^*}}{n\kappa} \lesssim \frac{\sigma\lambda\sqrt{s^*}}{n\kappa}.$$

In addition,

$$\begin{aligned}\|\hat{\beta} - \beta^*\|_{G,\tau} &= \sum_{i=1}^p \tau_i \|T^{(i)}\|_2 \leq (1+r) \sum_{i \in \mathcal{I}_*} \tau_i \|T^{(i)}\|_2 \\ &\leq (1+r) \frac{\sqrt{s^*} \|X(\hat{\beta} - \beta^*)\|_2}{\sqrt{n\kappa}} \leq (1+r) 2C \frac{\sigma \lambda s^*}{n\kappa^2} \lesssim \frac{\sigma \lambda s^*}{n\kappa^2},\end{aligned}$$

and

$$\|\hat{\beta} - \beta^*\|_2 = \left\| \sum_{i=1}^p \frac{1}{\tau_i} \tau_i T^{(i)} \right\|_2 \leq \frac{1}{\tau_{\min}} \sum_{i=1}^p \tau_i \|T^{(i)}\|_2 = \frac{1}{\tau_{\min}} \|\hat{\beta} - \beta^*\|_{G,\tau} \lesssim \frac{\sigma \lambda s^*}{n\kappa^2 \tau_{\min}}.$$

## E Proof of Theorem 2.2

**Proof.** Since  $\hat{\beta}$  is an optimal solution of problem (1.4), Theorem 2.1 has already indicated that  $\hat{\beta}$  is within a certain neighborhood of  $\beta^*$ . For  $u \in \mathbb{R}^p$ , define  $Q_n(u) = \sqrt{n} \|Xu/\sqrt{n} - \sigma\epsilon\|_2 + \lambda \|u/\sqrt{n} + \beta^*\|_{G,\tau}$ , then it is easy to check that

$$\hat{u} = \sqrt{n}(\hat{\beta} - \beta^*) = \arg \min_{u \in \mathbb{R}^p} Q_n(u).$$

Futhermore, we have

$$\begin{aligned}Q_n(u) - Q_n(0) &= \sqrt{n} \|Xu/\sqrt{n} - \sigma\epsilon\|_2 + \lambda \|u/\sqrt{n} + \beta^*\|_{G,\tau} - \sigma\sqrt{n} \|\epsilon\|_2 - \lambda \|\beta^*\|_{G,\tau} \\ &= \underbrace{\frac{1}{2\sigma} \left(\frac{\epsilon^\top \epsilon}{n}\right)^{-\frac{1}{2}} \left(\frac{1}{n} u^\top X^\top Xu - \frac{2\sigma}{\sqrt{n}} u^\top X^\top \epsilon\right)}_{I_1} - \underbrace{\frac{1}{2\sigma n} \left(\frac{\epsilon^\top \epsilon}{n}\right)^{-\frac{3}{2}} \cdot \frac{u^\top X^\top \epsilon \epsilon^\top Xu}{n}}_{I_2} \\ &\quad + \lambda \underbrace{\left(\|u/\sqrt{n} + \beta^*\|_{G,\tau} - \|\beta^*\|_{G,\tau}\right)}_{I_3} + o(\|u\|_2^2) \\ &=: I_1 + I_2 + I_3 + o(\|u\|_2^2).\end{aligned}$$

From Assumption 2.5 and Assumption 2.6, it follows that

$$I_1 \xrightarrow{d} \frac{1}{2\sigma} (u^\top Mu - 2u^\top W),$$

where  $W \sim N(0, \sigma^2 M)$ . Additionally, it is not difficult to see that as  $n \rightarrow \infty$ ,  $I_2 \rightarrow 0$ . Without loss of generality, we assume that the first  $s^*$  elements of  $\beta^*$  are nonzeros, and the remaining elements are zeros, i.e.,  $\beta^* = \begin{pmatrix} \beta_{\mathcal{I}_*}^* \\ 0 \end{pmatrix}$ . Hence,

$$\begin{aligned}I_3 &= \lambda \left( \left\| \begin{pmatrix} \frac{u_{\mathcal{I}_*}}{\sqrt{n}} + \beta_{\mathcal{I}_*}^* \\ \frac{u_{\mathcal{I}_c}}{\sqrt{n}} \end{pmatrix} \right\|_{G,\tau} - \left\| \begin{pmatrix} \beta_{\mathcal{I}_*}^* \\ 0 \end{pmatrix} \right\|_{G,\tau} \right) \\ &= \lambda \left( \underbrace{\left\| \begin{pmatrix} \frac{u_{\mathcal{I}_*}}{\sqrt{n}} + \beta_{\mathcal{I}_*}^* \\ 0 \end{pmatrix} \right\|_{G,\tau}}_{I_4} - \left\| \begin{pmatrix} \beta_{\mathcal{I}_*}^* \\ 0 \end{pmatrix} \right\|_{G,\tau} \right) + \underbrace{\frac{\lambda}{\sqrt{n}} \left\| \begin{pmatrix} 0 \\ u_{\mathcal{I}_c} \end{pmatrix} \right\|_{G,\tau}}_{I_5} \\ &=: I_4 + I_5.\end{aligned}$$

Denote  $V^{(1)}, V^{(2)}, \dots, V^{(p)}$  as an arbitrary optimal decomposition of  $u$ . Then, by the triangle inequality, we have

$$|I_4| \leq \frac{\lambda}{\sqrt{n}} \left\| \begin{pmatrix} u_{\mathcal{I}_*} \\ 0 \end{pmatrix} \right\|_{G, \tau} = \frac{\lambda}{\sqrt{n}} \sum_{i \in \mathcal{I}_*} \tau_i \|V^{(i)}\|_2. \quad (\text{A.10})$$

If  $\frac{\lambda}{\sqrt{n}} \rightarrow 0$  and  $\tau_i = O(1)$  for each  $i \in \mathcal{I}_*$ , then for each fixed  $u$ , we have  $|I_4| \rightarrow 0$  as  $n \rightarrow \infty$ . Furthermore, we observe that

$$|I_5| = \frac{\lambda}{\sqrt{n}} \sum_{i \in \mathcal{I}_*^c} \tau_i \|V^{(i)}\|_2 = (\lambda n^{(\nu-1)/2}) (n^{-\nu/2} \sum_{i \in \mathcal{I}_*^c} \tau_i \|V^{(i)}\|_2). \quad (\text{A.11})$$

If  $\lambda n^{(\nu-1)/2} \rightarrow \infty$ ,  $u_{\mathcal{I}_*^c} \neq 0$ , and  $\liminf_{n \rightarrow \infty} n^{-\nu/2} \tau_i > 0$  for each  $i \in \mathcal{I}_*^c$ , then  $I_5 \rightarrow \infty$  as  $n \rightarrow \infty$ . Hence, we get  $Q_n(u) - Q_n(0) \xrightarrow{d} D(u)$ , where

$$D(u) = \begin{cases} \frac{1}{2\sigma} (u^\top M u - 2u^\top W), & \text{if } \text{supp}(u) \subseteq \mathcal{I}_*, \\ \infty, & \text{else.} \end{cases}$$

Since  $\hat{u} = \arg \min_{u \in \mathbb{R}^p} Q_n(u) = \arg \min_{u \in \mathbb{R}^p} (Q_n(u) - Q_n(0))$  and  $u^* = (M_{\mathcal{I}_*, \mathcal{I}_*}^{-1} W_{\mathcal{I}_*}, 0)^\top = \arg \min_{u \in \mathbb{R}^p} D(u)$ , then by the argmax theorem [43, Corollary 3.2.3], we have  $\hat{u} \xrightarrow{d} u^*$ . Thus

$$\sqrt{n}(\hat{\beta}_{\mathcal{I}_*} - \beta_{\mathcal{I}_*}^*) \xrightarrow{d} N(0, \sigma^2 M_{\mathcal{I}_*, \mathcal{I}_*}^{-1}), \sqrt{n}\hat{\beta}_{\mathcal{I}_*^c} \xrightarrow{d} 0 \text{ and therefore } \hat{\beta}_{\mathcal{I}_*^c} \xrightarrow{p} 0.$$

## F Proof of Theorem 2.3

**Proof.** Assume that  $\hat{\beta}$  is an optimal solution of (1.4), then it follows from the triangle inequality that

$$\sigma \|\epsilon\|_2 - \|X(\hat{\beta} - \beta^*)\|_2 \leq \|y - X\hat{\beta}\|_2 \leq \sigma \|\epsilon\|_2 + \|X(\hat{\beta} - \beta^*)\|_2.$$

Based on the assumptions of Theorem 2.1, we obtain the following during its proof:

$$\|X(\hat{\beta} - \beta^*)\|_2 \leq \frac{C\sigma\lambda\sqrt{s^*}\|\epsilon\|_2}{n\kappa}, \text{ with } C = \frac{2r}{1 - \frac{\lambda^2 s^*}{n^2 \kappa^2}}.$$

Then we can get

$$\left(1 - \frac{C\lambda\sqrt{s^*}}{n\kappa}\right) \sigma \|\epsilon\|_2 \leq \|y - X\hat{\beta}\|_2 \leq \left(1 + \frac{C\lambda\sqrt{s^*}}{n\kappa}\right) \sigma \|\epsilon\|_2. \quad (\text{A.12})$$

The above expression implies that  $y \neq X\hat{\beta}$ . Therefore, we can conclude from Lemma 2.1 that  $\hat{\beta}$  can be decomposed as  $\hat{\beta} = \sum_{i=1}^p V^{(i)}$  where  $V^{(i)}$ 's satisfy that, for all  $1 \leq i \leq p$ ,

(a)  $V_{\mathcal{N}_i^c}^{(i)} = 0$ ;

(b) either  $V_{\mathcal{N}_i}^{(i)} \neq 0$  and  $\frac{X_{\mathcal{N}_i}^\top (y - X\hat{\beta})}{\|y - X\hat{\beta}\|_2} = \frac{\lambda\tau_i V_{\mathcal{N}_i}^{(i)}}{\sqrt{n}\|V_{\mathcal{N}_i}^{(i)}\|_2}$ , or  $V_{\mathcal{N}_i}^{(i)} = 0$  and  $\frac{\|X_{\mathcal{N}_i}^\top (y - X\hat{\beta})\|_2}{\|y - X\hat{\beta}\|_2} \leq \frac{\lambda\tau_i}{\sqrt{n}}$ .

Denote  $\hat{H} = \{i : \|V_{\mathcal{N}_i}^{(i)}\|_2 \neq 0\}$ . For  $i \in \hat{H}$ ,  $\frac{X_{\mathcal{N}_i}^\top (y - X\hat{\beta})}{\|y - X\hat{\beta}\|_2} = \frac{\lambda\tau_i V_{\mathcal{N}_i}^{(i)}}{\sqrt{n}\|V_{\mathcal{N}_i}^{(i)}\|_2}$ . For  $i \notin \hat{H}$ ,  $\frac{X_{\mathcal{N}_i}^\top (y - X\hat{\beta})}{\|y - X\hat{\beta}\|_2} = \frac{\lambda\tau_i}{\sqrt{n}} Z_{\mathcal{N}_i}^{(i)}$ , where  $Z^{(i)}$  is  $p \times 1$  random vectors with  $\|Z_{\mathcal{N}_i}^{(i)}\|_2 \leq 1$ . Since some predictors may belong to multiple

neighborhoods, the following conditions need to be satisfied:

- (i)  $\tau_{i_1} V_i^{(i_1)} / \|V_{\mathcal{N}_{i_1}^{(i_1)}}\|_2 = \tau_{i_2} V_i^{(i_2)} / \|V_{\mathcal{N}_{i_2}^{(i_2)}}\|_2$  for each  $i_1 \in \hat{H}$ ,  $i_2 \in \hat{H}$ , and  $i \in \mathcal{N}_{i_1} \cap \mathcal{N}_{i_2}$ .
- (ii)  $\tau_{i_1} V_i^{(i_1)} / \|V_{\mathcal{N}_{i_1}^{(i_1)}}\|_2 = \tau_{i_2} Z_i^{(i_2)}$  for each  $i_1 \in \hat{H}$ ,  $i_2 \notin \hat{H}$ , and  $i \in \mathcal{N}_{i_1} \cap \mathcal{N}_{i_2}$ .
- (iii)  $\tau_{i_1} Z_i^{(i_1)} = \tau_{i_2} Z_i^{(i_2)}$  for each  $i_1 \notin \hat{H}$ ,  $i_2 \notin \hat{H}$ , and  $i \in \mathcal{N}_{i_1} \cap \mathcal{N}_{i_2}$ .

Then, we can get any solution  $\hat{\beta}$  satisfies the following equation

$$\frac{X^\top (y - X\hat{\beta})}{\|y - X\hat{\beta}\|_2} = \frac{\lambda}{\sqrt{n}} \hat{f},$$

where for  $i \in \hat{H}$ ,  $\hat{f}_i = \tau_i V_i^{(i)} / \|V_{\mathcal{N}_i^{(i)}}\|_2$ . And for  $i \notin \hat{H}$ ,  $\hat{f}_i = \tau_i Z_i^{(i)}$ . Define  $\hat{\psi} := \|y - X\hat{\beta}\|_2$ , then the above equation is transformed as

$$X^\top (y - X\hat{\beta}) = \frac{\lambda \hat{\psi} \hat{f}}{\sqrt{n}}. \quad (\text{A.13})$$

Define  $\Omega_1 := \{\|\hat{\beta}_{\mathcal{I}_*} - \beta_{\mathcal{I}_*}^*\|_\infty < \beta_{min}^*\}$ ,  $\Omega_2 := \{\|\hat{f}_{\mathcal{N}_i}\|_2 < \tau_i \text{ for each } i \in \mathcal{I}_*^c\}$ . If event  $\Omega_1$  occurs, then  $\text{sign}(\hat{\beta}_i) = \text{sign}(\beta_i^*)$  for each  $i \in \mathcal{I}_*$ . If event  $\Omega_2$  occurs, then  $V_{\mathcal{N}_i}^{(i)} = 0$  for each  $i \in \mathcal{I}_*^c$ . Furthermore, based on  $V_{\mathcal{N}_i^c}^{(i)} = 0$  for each  $i$  and Assumption 2.2, we can derive  $\hat{\beta}_{\mathcal{I}_*^c} = \sum_{i \in \mathcal{I}_*^c} V_{\mathcal{I}_*^c}^{(i)} = 0$ . Therefore, if we can prove  $\mathbb{P}(\Omega_1 \cap \Omega_2) \rightarrow 1$ , we can obtain  $\mathbb{P}(\text{sign}(\hat{\beta}) = \text{sign}(\beta^*)) \rightarrow 1$  as  $n \rightarrow \infty$ .

Note that if events  $\Omega_1$  and  $\Omega_2$  occur, then equation (A.13) yields that

$$X_{\mathcal{I}_*}^\top (X_{\mathcal{I}_*} \beta_{\mathcal{I}_*}^* + \sigma \epsilon - X_{\mathcal{I}_*} \hat{\beta}_{\mathcal{I}_*}) = \frac{\lambda \hat{\psi} \hat{f}_{\mathcal{I}_*}}{\sqrt{n}};$$

$$X_{\mathcal{N}_i}^\top (X_{\mathcal{I}_*} \beta_{\mathcal{I}_*}^* + \sigma \epsilon - X_{\mathcal{I}_*} \hat{\beta}_{\mathcal{I}_*}) = \frac{\lambda \hat{\psi} \hat{f}_{\mathcal{N}_i}}{\sqrt{n}} \text{ for each } i \in \mathcal{I}_*^c.$$

Thus,

$$\hat{\beta}_{\mathcal{I}_*} - \beta_{\mathcal{I}_*}^* = \sigma (X_{\mathcal{I}_*}^\top X_{\mathcal{I}_*})^{-1} X_{\mathcal{I}_*}^\top \epsilon - \frac{\lambda \hat{\psi}}{\sqrt{n}} (X_{\mathcal{I}_*}^\top X_{\mathcal{I}_*})^{-1} \hat{f}_{\mathcal{I}_*}, \quad (\text{A.14})$$

$$\frac{\hat{f}_{\mathcal{N}_i}}{\tau_i} = \frac{\sigma \sqrt{n}}{\lambda \hat{\psi} \tau_i} X_{\mathcal{N}_i}^\top (I_n - X_{\mathcal{I}_*} (X_{\mathcal{I}_*}^\top X_{\mathcal{I}_*})^{-1} X_{\mathcal{I}_*}^\top) \epsilon + \frac{1}{\tau_i} X_{\mathcal{N}_i}^\top X_{\mathcal{I}_*} (X_{\mathcal{I}_*}^\top X_{\mathcal{I}_*})^{-1} \hat{f}_{\mathcal{I}_*}. \quad (\text{A.15})$$

Firstly, from (A.14), we have

$$\begin{aligned} \|\hat{\beta}_{\mathcal{I}_*} - \beta_{\mathcal{I}_*}^*\|_\infty &\leq \sigma \|(X_{\mathcal{I}_*}^\top X_{\mathcal{I}_*})^{-1} X_{\mathcal{I}_*}^\top \epsilon\|_\infty + \frac{\lambda \hat{\psi}}{n^{3/2}} \left\| \left( \frac{X_{\mathcal{I}_*}^\top X_{\mathcal{I}_*}}{n} \right)^{-1} \hat{f}_{\mathcal{I}_*} \right\|_\infty \\ &\leq \sigma \|(X_{\mathcal{I}_*}^\top X_{\mathcal{I}_*})^{-1} X_{\mathcal{I}_*}^\top \epsilon\|_\infty + \frac{\lambda \hat{\psi}}{n^{3/2}} \left\| \left( \frac{X_{\mathcal{I}_*}^\top X_{\mathcal{I}_*}}{n} \right)^{-1} \right\|_\infty \|\hat{f}_{\mathcal{I}_*}\|_\infty. \end{aligned}$$

By (A.12), Assumption 2.9 and Lemma 4.2, we can get

$$\begin{aligned}
\|\hat{\beta}_{\mathcal{I}_*} - \beta_{\mathcal{I}_*}^*\|_\infty &\leq \sigma \|(X_{\mathcal{I}_*}^\top X_{\mathcal{I}_*})^{-1} X_{\mathcal{I}_*}^\top \epsilon\|_\infty + \frac{\lambda}{n^{3/2}} \left(1 + \frac{C\lambda\sqrt{s^*}}{n\kappa}\right) \sigma \|\epsilon\|_2 \frac{\sqrt{s^*}}{Q_2} \|\hat{f}_{\mathcal{I}_*}\|_\infty \\
&\leq \sigma \|(X_{\mathcal{I}_*}^\top X_{\mathcal{I}_*})^{-1} X_{\mathcal{I}_*}^\top \epsilon\|_\infty + \frac{2\sigma\lambda\sqrt{s^*}}{nQ_2} \left(1 + \frac{C\lambda\sqrt{s^*}}{n\kappa}\right) \|\hat{f}_{\mathcal{I}_*}\|_\infty \\
&\leq \sigma \|(X_{\mathcal{I}_*}^\top X_{\mathcal{I}_*})^{-1} X_{\mathcal{I}_*}^\top \epsilon\|_\infty + \frac{2\sigma\lambda\sqrt{s^*}}{nQ_2} \left(1 + \frac{C\lambda\sqrt{s^*}}{n\kappa}\right) \max_{i \in \mathcal{I}_*} \tau_i,
\end{aligned}$$

where the last inequality is due to  $|\hat{f}_i| \leq \tau_i$  for each  $i$ . Then, by Markov inequality, we have

$$\begin{aligned}
\mathbb{P}(\|\hat{\beta}_{\mathcal{I}_*} - \beta_{\mathcal{I}_*}^*\|_\infty \geq \beta_{min}^*) &\leq \frac{E(\|\hat{\beta}_{\mathcal{I}_*} - \beta_{\mathcal{I}_*}^*\|_\infty)}{\beta_{min}^*} \\
&\leq \frac{1}{\beta_{min}^*} \left( E(\|\sigma(X_{\mathcal{I}_*}^\top X_{\mathcal{I}_*})^{-1} X_{\mathcal{I}_*}^\top \epsilon\|_\infty) + \frac{2\sigma\lambda\sqrt{s^*}}{nQ_2} \left(1 + \frac{C\lambda\sqrt{s^*}}{n\kappa}\right) \max_{i \in \mathcal{I}_*} \tau_i \right).
\end{aligned}$$

It is easy to see that  $\sigma(X_{\mathcal{I}_*}^\top X_{\mathcal{I}_*})^{-1} X_{\mathcal{I}_*}^\top \epsilon$  follows the multivariate normal distribution with mean 0 and covariance matrix  $\sigma^2(X_{\mathcal{I}_*}^\top X_{\mathcal{I}_*})^{-1}$ . Using standard results on the maximum of this Gaussian vector [28], we have

$$E(\|\sigma(X_{\mathcal{I}_*}^\top X_{\mathcal{I}_*})^{-1} X_{\mathcal{I}_*}^\top \epsilon\|_\infty) \leq 3\sigma \sqrt{\frac{\log s^*}{nQ_2}}.$$

Hence,

$$\mathbb{P}(\|\hat{\beta}_{\mathcal{I}_*} - \beta_{\mathcal{I}_*}^*\|_\infty \geq \beta_{min}^*) \leq \frac{1}{\beta_{min}^*} \left( 3\sigma \sqrt{\frac{\log s^*}{nQ_2}} + \frac{2\sigma\lambda\sqrt{s^*}}{nQ_2} \left(1 + \frac{C\lambda\sqrt{s^*}}{n\kappa}\right) \max_{i \in \mathcal{I}_*} \tau_i \right) \rightarrow 0 \text{ as } n \rightarrow \infty.$$

We conclude

$$\mathcal{P}(\Omega_1) \rightarrow 1 \text{ as } n \rightarrow \infty. \tag{A.16}$$

Next, we will prove  $\mathcal{P}(\Omega_2) \rightarrow 1$  as  $n \rightarrow \infty$ . For each  $i \in \mathcal{I}_*^c$ , from (A.15), we can get

$$\begin{aligned}
\frac{\|\hat{f}_{\mathcal{N}_i}\|_2}{\tau_i} &\leq \frac{\sigma\sqrt{n}}{\lambda\hat{\psi}\tau_i} \|X_{\mathcal{N}_i}^\top (I_n - X_{\mathcal{I}_*} (X_{\mathcal{I}_*}^\top X_{\mathcal{I}_*})^{-1} X_{\mathcal{I}_*}^\top) \epsilon\|_2 \\
&\quad + \frac{1}{\tau_i} \|X_{\mathcal{N}_i}^\top X_{\mathcal{I}_*} (X_{\mathcal{I}_*}^\top X_{\mathcal{I}_*})^{-1} \hat{f}_{\mathcal{I}_*}\|_2 \\
&\leq \frac{\sigma\sqrt{n}\sqrt{d_i}}{\lambda\hat{\psi}\tau_i} \|X_{\mathcal{N}_i}^\top (I_n - X_{\mathcal{I}_*} (X_{\mathcal{I}_*}^\top X_{\mathcal{I}_*})^{-1} X_{\mathcal{I}_*}^\top) \epsilon\|_\infty \\
&\quad + \frac{\sqrt{d_i}\sqrt{s^*}}{\tau_i} \|X_{\mathcal{N}_i}^\top X_{\mathcal{I}_*} (X_{\mathcal{I}_*}^\top X_{\mathcal{I}_*})^{-1}\|_\infty \max_{i \in \mathcal{I}_*} \tau_i \\
&\leq \frac{\sqrt{2d_i}}{\lambda\tau_i(1 - \frac{C\lambda\sqrt{s^*}}{n\kappa})} \|X_{\mathcal{N}_i}^\top (I_n - X_{\mathcal{I}_*} (X_{\mathcal{I}_*}^\top X_{\mathcal{I}_*})^{-1} X_{\mathcal{I}_*}^\top) \epsilon\|_\infty \\
&\quad + \frac{\sqrt{d_i}\sqrt{s^*}}{\tau_i} \|X_{\mathcal{N}_i}^\top X_{\mathcal{I}_*} (X_{\mathcal{I}_*}^\top X_{\mathcal{I}_*})^{-1}\|_\infty \max_{i \in \mathcal{I}_*} \tau_i \\
&\leq \frac{\sqrt{2d_i}}{\lambda\tau_i(1 - \frac{C\lambda\sqrt{s^*}}{n\kappa})} \|X_{\mathcal{N}_i}^\top (I_n - X_{\mathcal{I}_*} (X_{\mathcal{I}_*}^\top X_{\mathcal{I}_*})^{-1} X_{\mathcal{I}_*}^\top) \epsilon\|_\infty \\
&\quad + \frac{(1 - \xi)\sqrt{d_i}\sqrt{s^*} \max_{i \in \mathcal{I}_*} \tau_i}{\tau_i},
\end{aligned}$$

where the last inequality follows from Assumption 2.10. Thus, we have

$$\max_{i \in \mathcal{I}_*^c} \frac{\|\hat{f}_{\mathcal{N}_i}\|_2}{\tau_i} \leq \frac{\sqrt{2}}{\lambda(1 - \frac{C\lambda\sqrt{s^*}}{n\kappa}) \min_{i \in \mathcal{I}_*^c} m_i} \|X_{\mathcal{I}_*^c}^\top (I_n - X_{\mathcal{I}_*} (X_{\mathcal{I}_*}^\top X_{\mathcal{I}_*})^{-1} X_{\mathcal{I}_*}^\top) \epsilon\|_\infty + \frac{(1 - \xi)s^* \max_{i \in \mathcal{I}_*} m_i}{\min_{i \in \mathcal{I}_*^c} m_i}.$$

We observe that  $X_{\mathcal{I}_*^c}^\top (I_n - X_{\mathcal{I}_*} (X_{\mathcal{I}_*}^\top X_{\mathcal{I}_*})^{-1} X_{\mathcal{I}_*}^\top) \epsilon$  follows a multivariate normal distribution with mean 0 and covariance matrix  $X_{\mathcal{I}_*^c}^\top (I_n - X_{\mathcal{I}_*} (X_{\mathcal{I}_*}^\top X_{\mathcal{I}_*})^{-1} X_{\mathcal{I}_*}^\top) X_{\mathcal{I}_*^c}$ . By the Assumption 2.8, the variance of each component is bounded by  $nQ_1^2$ . Thus, by the Markov inequality and the result on the maximum of this Gaussian vector, we have

$$\begin{aligned}
&\mathbb{P}\left(\frac{\sqrt{2}}{\lambda(1 - \frac{C\lambda\sqrt{s^*}}{n\kappa}) \min_{i \in \mathcal{I}_*^c} m_i} \|X_{\mathcal{I}_*^c}^\top (I_n - X_{\mathcal{I}_*} (X_{\mathcal{I}_*}^\top X_{\mathcal{I}_*})^{-1} X_{\mathcal{I}_*}^\top) \epsilon\|_\infty > \xi\right) \\
&\leq \frac{3\sqrt{2}Q_1}{\lambda\xi(1 - \frac{C\lambda\sqrt{s^*}}{n\kappa}) \min_{i \in \mathcal{I}_*^c} m_i} \sqrt{\frac{\log(p - s^*)}{n}} \rightarrow 0 \text{ as } n \rightarrow \infty.
\end{aligned}$$

Furthermore, By Assumption 2.7, if  $m_i$ 's satisfy that  $\liminf_{n \rightarrow \infty} n^{-\varsigma} \min_{i \in \mathcal{I}_*^c} m_i > 0$  for some  $\varsigma > \delta_0$  and  $\max_{i \in \mathcal{I}_*} m_i = O_p(1)$ , there is

$$\frac{(1 - \xi)s^* \max_{i \in \mathcal{I}_*} m_i}{\min_{i \in \mathcal{I}_*^c} m_i} = (1 - \xi) \frac{s^* \max_{i \in \mathcal{I}_*} m_i}{n^\varsigma n^{-\varsigma} \min_{i \in \mathcal{I}_*^c} m_i} \rightarrow 0 \text{ as } n \rightarrow \infty.$$

Thus,

$$\mathbb{P}(\Omega_2) = \mathbb{P}\left(\max_{i \in \mathcal{I}_c^c} \frac{\|\hat{f}_{\mathcal{N}_i}\|_2}{\tau_i} < 1\right) \rightarrow 1 \text{ as } n \rightarrow \infty. \quad (\text{A.17})$$

By (A.16) and (A.17), we conclude that  $\mathcal{P}(\Omega_1 \cap \Omega_2) \rightarrow 1$  and  $\mathbb{P}(\text{sign}(\hat{\beta}) = \text{sign}(\beta^*)) \rightarrow 1$  as  $n \rightarrow \infty$ .

## G Proof of Lemma 3.1

**Proof.** From the so-called Moreau decomposition, we can get  $\text{Prox}_f(x) = x - \text{Prox}_{f^*}(x)$ . Therefore, we first derive the expression of  $f^*$ :

$$\begin{aligned} f^*(z) &= \sup_{v \in \mathbb{R}^p} \left\{ \langle z, v \rangle - \frac{\lambda}{\sigma n} \|v\|_{G, \tau} \right\} \\ &= \sup_{v \in \mathbb{R}^p} \left\{ \langle z, v \rangle - \min_{\sum_{i=1}^p V^{(i)}=v, \text{supp}(V^{(i)}) \subseteq \mathcal{N}_i} \frac{\lambda}{\sigma n} \sum_{i=1}^p \tau_i \|V^{(i)}\|_2 \right\} \\ &= \sup_{v \in \mathbb{R}^p} \left\{ \sup_{\sum_{i=1}^p V^{(i)}=v} \left\{ \langle z, v \rangle - \frac{\lambda}{\sigma n} \sum_{i=1}^p \tau_i \|V_{\mathcal{N}_i}^{(i)}\|_2 \right\} \right\} \\ &= \sup_{V_{\mathcal{N}_i}^{(i)} \in \mathbb{R}^{|\mathcal{N}_i|}} \left\{ \langle z_{\mathcal{N}_i}, \sum_{i=1}^p V_{\mathcal{N}_i}^{(i)} \rangle - \sum_{i=1}^p \frac{\lambda \tau_i}{\sigma n} \|V_{\mathcal{N}_i}^{(i)}\|_2 \right\} \\ &= \sum_{i=1}^p \sup_{V_{\mathcal{N}_i}^{(i)} \in \mathbb{R}^{|\mathcal{N}_i|}} \left\{ \langle z_{\mathcal{N}_i}, V_{\mathcal{N}_i}^{(i)} \rangle - \frac{\lambda \tau_i}{\sigma n} \|V_{\mathcal{N}_i}^{(i)}\|_2 \right\} \\ &= \sum_{i=1}^p \delta_{B_2^{\frac{\lambda \tau_i}{\sigma n}}}(z_{\mathcal{N}_i}), \end{aligned}$$

where  $B_2^{\frac{\lambda \tau_i}{\sigma n}} := \{x \mid \|x\|_2 \leq \frac{\lambda \tau_i}{\sigma n}\}$ . The validity of the last equation is due to the fact that the conjugate function of  $\ell_2$  norm is the indicator function of its dual norm unit ball. Furthermore, we obtain that  $\sum_{i=1}^p \delta_{B_2^{\frac{\lambda \tau_i}{\sigma n}}}(z_{\mathcal{N}_i}) = \delta_{\mathcal{S}_\circ}(z)$  by [44, lemma2]. Then, based on the definition of proximal point mapping, we can get

$$\text{Prox}_{f^*}(x) = \arg \min_{z \in \mathbb{R}^p} \left\{ \delta_{\mathcal{S}_\circ}(z) + \frac{1}{2} \|z - x\|_2^2 \right\} = \arg \min_{z \in \mathcal{S}_\circ} \frac{1}{2} \|z - x\|_2^2 = \Pi_{\mathcal{S}_\circ}(x).$$

So far, the conclusion of this lemma has been proved.

## References

- [1] A. Beck. *First-order methods in optimization*. 2017.
- [2] P. Bellec, G. Lecué, and A. Tsybakov. Slope meets lasso: improved oracle bounds and optimality. *The Annals of Statistics*, 46(6B):3603–3642, 2018.
- [3] A. Belloni, V. Chernozhukov, and L. Wang. Square-root lasso: pivotal recovery of sparse signals via conic programming. *Biometrika*, 98(4):791–806, 2011.

- [4] P. Bickel, Y. Ritov, and A. Tsybakov. Simultaneous analysis of Lasso and Dantzig selector. *The Annals of Statistics*, 37(4):1705–1732, 2009.
- [5] H. Bondell and B. Reich. Simultaneous regression shrinkage, variable selection, and supervised clustering of predictors with OSCAR. *Biometrics*, 64(1):115–123, 2008.
- [6] O. Bousquet. A Bennett concentration inequality and its application to suprema of empirical processes. *Comptes Rendus Mathématique*, 334(6):495–500, 2002.
- [7] P. Bühlmann and S. Van De Geer. *Statistics for high-dimensional data: methods, theory and applications*. 2011.
- [8] F. Bunea, J. Lederer, and Y. She. The group square-root lasso: Theoretical properties and fast algorithms. *IEEE Transactions on Information Theory*, 60(2):1313–1325, 2013.
- [9] T. Cai, W. Liu, and X. Luo. A constrained  $\ell_1$  minimization approach to sparse precision matrix estimation. *Journal of the American Statistical Association*, 106(494):594–607, 2011.
- [10] P. Combettes and J. Pesquet. Proximal splitting methods in signal processing. *Fixed-point algorithms for inverse problems in science and engineering*, pages 185–212, 2011.
- [11] Y. Cui, J. Pang, and B. Sen. Composite difference-max programs for modern statistical estimation problems. *SIAM Journal on Optimization*, 28(4):3344–3374, 2018.
- [12] A. Derumigny. Improved bounds for square-root lasso and square-root slope. *Electronic Journal of Statistics*, 12(1):741–766, 2018.
- [13] Y. Ding, H. Zhang, P. Li, and Y. Xiao. An efficient semismooth Newton method for adaptive sparse signal recovery problems. *Optimization Methods and Software*, 38(2):262–288, 2023.
- [14] J. Fan and R. Li. Variable selection via nonconcave penalized likelihood and its oracle properties. *Journal of the American Statistical Association*, 96(456):1348–1360, 2001.
- [15] M. Fazel, T. Pong, D. Sun, and P. Tseng. Hankel matrix rank minimization with applications to system identification and realization. *SIAM Journal on Matrix Analysis and Applications*, 34(3):946–977, 2013.
- [16] L. Frank and J. Friedman. A statistical view of some chemometrics regression tools. *Technometrics*, 35(2):109–135, 1993.
- [17] J. Friedman. Multivariate adaptive regression splines. *The Annals of Statistics*, 19(1):1–67, 1991.
- [18] J. Friedman, T. Hastie, and R. Tibshirani. Sparse inverse covariance estimation with the graphical lasso. *Biostatistics*, 9(3):432–441, 2008.
- [19] R. Garzon, G. Calin, and C. Croce. MicroRNAs in cancer. *Annual Review of Medicine*, 60:167–179, 2009.
- [20] G. Golub and C. Van Loan. *Matrix computations*. 2013.
- [21] J. Hayes, P. Peruzzi, and S. Lawler. MicroRNAs in cancer: biomarkers, functions and therapy. *Trends in Molecular Medicine*, 20(8):460–469, 2014.
- [22] L. Huang, J. Jia, B. Yu, B. Chun, P. Maniatis, and M. Naik. Predicting execution time of computer programs using sparse polynomial regression. *Advances in neural information processing systems*, 2010.

- [23] S. Kim and E. Xing. Statistical estimation of correlated genome associations to a quantitative trait network. *PLoS Genetics*, 5(8):e1000587, 2009.
- [24] V. Koltchinskii and M. Yuan. Sparsity in multiple kernel learning. *The Annals of Statistics*, 38(6):3660–3695, 2010.
- [25] Y. Kong, D. Ferland-McCollough, T. Jackson, and M. Bushell. MicroRNAs in cancer management. *The Lancet Oncology*, 13(6):e249–e258, 2012.
- [26] B. Laurent and P. Massart. Adaptive estimation of a quadratic functional by model selection. *The Annals of Statistics*, 28(5):1302–1338, 2000.
- [27] J. Lederer and S. Van De Geer. New concentration inequalities for empirical processes. *Bernoulli*, 2011.
- [28] M. Ledoux and M. Talagrand. *Probability in Banach Spaces: isoperimetry and processes*. 2013.
- [29] C. Li and H. Li. Network-constrained regularization and variable selection for analysis of genomic data. *Bioinformatics*, 24(9):1175–1182, 2008.
- [30] J. Liu, G. Yu, and Y. Liu. Graph-based sparse linear discriminant analysis for high-dimensional classification. *Journal of Multivariate Analysis*, 171:250–269, 2019.
- [31] K. Lounici, M. Pontil, S. Van De Geer, and A. Tsybakov. Oracle inequalities and optimal inference under group sparsity. *The Annals of Statistics*, 39(4):2164–2204, 2011.
- [32] Y. Luo and Y. Liu. Recovery of sums of sparse and dense signals by incorporating graphical structure among predictors. *Canadian Journal of Statistics*, 50(2):471–490, 2022.
- [33] L. Meier, S. Van De Geer, and P. Bühlmann. High-dimensional additive modeling. *The Annals of Statistics*, 37(6B):3779–3821, 2009.
- [34] G. Obozinski, L. Jacob, and J. Vert. Group lasso with overlaps: the latent group lasso approach. *arXiv preprint arXiv:1110.0413*, 2011.
- [35] A. Owen. A robust hybrid of lasso and ridge regression. *Contemporary Mathematics*, 443(7):59–72, 2007.
- [36] Y. Pan, X. Zhao, S. Wei, and Z. Liu. High-dimensional expectile regression incorporating graphical structure among predictors. *Journal of Statistical Computation and Simulation*, 93(2):231–248, 2023.
- [37] X. Shen, L. Chen, Y. Gu, and H. So. Square-root lasso with nonconvex regularization: An ADMM approach. *IEEE Signal Processing Letters*, 23(7):934–938, 2016.
- [38] M. Stephenson, R. Ayesha Ali, G. Darlington, F. Schenkel, and E. Squires. DSLRIG: Leveraging predictor structure in logistic regression. *Communications in Statistics-Simulation and Computation*, 50(6):1600–1612, 2021.
- [39] A. Subramanian, P. Tamayo, V. Mootha, et al. Gene set enrichment analysis: a knowledge-based approach for interpreting genome-wide expression profiles. *Proceedings of the National Academy of Sciences*, 102(43):15545–15550, 2005.
- [40] P. Tang, C. Wang, D. Sun, and K. Toh. A sparse semismooth Newton based proximal majorization-minimization algorithm for nonconvex square-root-loss regression problems. *Journal of Machine Learning Research*, 21(226):1–38, 2020.

- [41] R. Tibshirani. Regression shrinkage and selection via the lasso. *Journal of the Royal Statistical Society: Series B (Methodological)*, 58(1):267–288, 1996.
- [42] S. Van De Geer and J. Lederer. The Bernstein-Orlicz norm and deviation inequalities. *Probability theory and related fields*, 157(1):225–250, 2013.
- [43] A. Van Der Vaart and J. Wellner. *Weak convergence and empirical processes: with applications to statistics*, volume 160. 1997.
- [44] S. Villa, L. Rosasco, S. Mosci, and A. Verri. Proximal methods for the latent group lasso penalty. *Computational Optimization and Applications*, 58:381–407, 2014.
- [45] L. Wang. The L1 penalized LAD estimator for high dimensional linear regression. *Journal of Multivariate Analysis*, 120:135–151, 2013.
- [46] Z. Wang, X. Liu, W. Tang, and Y. Lin. Incorporating graphical structure of predictors in sparse quantile regression. *Journal of Business & Economic Statistics*, 39(3):783–792, 2021.
- [47] Y. Wen, W. Ching, and M. Ng. A semi-smooth Newton method for inverse problem with uniform noise. *Journal of Scientific Computing*, 75(2):713–732, 2018.
- [48] X. Xiu, L. Kong, Y. Li, and H. Qi. Iterative reweighted methods for  $\ell_1 - \ell_p$  minimization. *Computational Optimization and Applications*, 70(1):201–219, 2018.
- [49] S. Yang, L. Yuan, Y. Lai, X. Shen, P. Wonka, and J. Ye. Feature grouping and selection over an undirected graph. In *Proceedings of the 18th ACM SIGKDD international conference on Knowledge discovery and data mining*, pages 922–930, 2012.
- [50] G. Yu and Y. Liu. Sparse regression incorporating graphical structure among predictors. *Journal of the American Statistical Association*, 111(514):707–720, 2016.
- [51] M. Yuan and Y. Lin. Model selection and estimation in regression with grouped variables. *Journal of the Royal Statistical Society: Series B (Methodological)*, 68(1):49–67, 2006.
- [52] M. Yuan and Y. Lin. Model selection and estimation in the Gaussian graphical model. *Biometrika*, 94(1):19–35, 2007.
- [53] C. Zhang. Nearly unbiased variable selection under minimax concave penalty. *The Annals of Statistics*, 38(2):894–942, 2010.
- [54] Z. Zhang and W. Wei. Primal-dual approach for uniform noise removal. In *First International Conference on Information Science and Electronic Technology (ISET 2015)*, pages 103–106, 2015.
- [55] P. Zhao and B. Yu. On model selection consistency of Lasso. *The Journal of Machine Learning Research*, 7:2541–2563, 2006.
- [56] S. Zhou, J. Zhou, and B. Zhang. High-dimensional generalized linear models incorporating graphical structure among predictors. *Electronic Journal of Statistics*, 13(2):3161–3194, 2019.

Table 1: Performance comparison of estimation, prediction and model selection for Example 1&2 with normal distribution noise.

Example 1										Example 2									
	$L_2$ distance	RPE	FPR	FNR	$L_2$ distance	RPE	FPR	FNR	FNR		$L_2$ distance	RPE	FPR	FNR	FNR				
(I) 20/20/400	Ridge	8.177(0.726)	7.130(2.433)	0.966(0.016)	0.000(0.000)	8.848(0.617)	7.700(1.952)	0.967(0.013)	0.001(0.009)		8.848(0.617)	7.700(1.952)	0.967(0.013)	0.001(0.009)					
	Lasso	12.899(1.820)	4.380(3.754)	0.097(0.023)	0.511(0.120)	11.390(1.230)	6.241(3.121)	0.092(0.020)	0.507(0.117)		11.390(1.230)	6.241(3.121)	0.092(0.020)	0.507(0.117)					
	Alasso	12.504(1.616)	3.253(2.356)	0.081(0.021)	0.441(0.105)	11.246(1.326)	5.248(2.820)	0.080(0.019)	0.440(0.104)		11.246(1.326)	5.248(2.820)	0.080(0.019)	0.440(0.104)					
	Enet	6.930(1.193)	5.419(2.932)	0.435(0.050)	0.011(0.034)	8.119(1.046)	6.954(2.435)	0.430(0.049)	0.036(0.069)		8.119(1.046)	6.954(2.435)	0.430(0.049)	0.036(0.069)					
	SRL	12.558(1.768)	3.842(2.837)	0.103(0.028)	0.464(0.110)	11.172(1.524)	5.836(3.588)	0.099(0.029)	0.439(0.118)		11.172(1.524)	5.836(3.588)	0.099(0.029)	0.439(0.118)					
	SRIG-o	8.773(0.656)	13.543(2.324)	0.565(0.063)	0.000(0.000)	9.305(0.513)	12.236(1.691)	0.565(0.058)	0.007(0.031)		9.305(0.513)	12.236(1.691)	0.565(0.058)	0.007(0.031)					
	SRIG	8.818(0.647)	13.702(2.324)	0.567(0.061)	0.000(0.000)	9.235(0.518)	12.060(1.691)	0.564(0.056)	0.009(0.049)		9.235(0.518)	12.060(1.691)	0.564(0.056)	0.009(0.049)					
	GSRE-o	3.638(1.470)	2.110(3.027)	0.022(0.020)	0.000(0.000)	4.817(1.513)	2.856(3.030)	0.023(0.022)	0.013(0.066)		4.817(1.513)	2.856(3.030)	0.023(0.022)	0.013(0.066)					
	GSRE	3.426(1.301)	1.888(2.525)	0.025(0.023)	0.000(0.000)	4.775(1.531)	2.856(3.056)	0.023(0.021)	0.013(0.066)		4.775(1.531)	2.856(3.056)	0.023(0.021)	0.013(0.066)					
	(II) 40/40/400	Ridge	6.972(0.614)	3.640(1.045)	0.960(0.015)	0.000(0.000)	7.334(0.581)	3.798(0.790)	0.966(0.013)	0.000(0.000)		7.334(0.581)	3.798(0.790)	0.966(0.013)	0.000(0.000)				
Lasso		9.181(1.344)	1.567(0.699)	0.056(0.018)	0.251(0.091)	7.722(1.277)	2.359(1.100)	0.045(0.019)	0.192(0.104)		7.722(1.277)	2.359(1.100)	0.045(0.019)	0.192(0.104)					
Alasso		9.448(1.388)	1.030(0.434)	0.049(0.018)	0.245(0.090)	7.771(1.337)	1.573(0.712)	0.040(0.018)	0.180(0.091)		7.771(1.337)	1.573(0.712)	0.040(0.018)	0.180(0.091)					
Enet		5.330(0.692)	4.007(1.321)	0.310(0.054)	0.000(0.000)	6.008(0.744)	4.223(1.269)	0.316(0.045)	0.005(0.018)		6.008(0.744)	4.223(1.269)	0.316(0.045)	0.005(0.018)					
SRL		9.098(1.343)	1.455(0.646)	0.067(0.025)	0.243(0.085)	7.607(1.283)	2.274(1.042)	0.051(0.027)	0.180(0.096)		7.607(1.283)	2.274(1.042)	0.051(0.027)	0.180(0.096)					
SRIG-o		3.312(1.136)	1.778(1.779)	0.031(0.058)	0.000(0.000)	4.120(1.335)	2.325(2.080)	0.054(0.076)	0.000(0.000)		4.120(1.335)	2.325(2.080)	0.054(0.076)	0.000(0.000)					
SRIG		3.118(1.180)	1.737(1.726)	0.031(0.059)	0.000(0.000)	3.860(1.184)	1.999(1.724)	0.044(0.065)	0.000(0.000)		3.860(1.184)	1.999(1.724)	0.044(0.065)	0.000(0.000)					
GSRE-o		2.487(0.505)	0.667(0.439)	0.012(0.013)	0.000(0.000)	3.041(0.594)	0.783(0.505)	0.016(0.013)	0.000(0.000)		3.041(0.594)	0.783(0.505)	0.016(0.013)	0.000(0.000)					
GSRE		2.385(0.529)	0.659(0.446)	0.013(0.013)	0.000(0.000)	3.007(0.576)	0.775(0.464)	0.016(0.013)	0.000(0.000)		3.007(0.576)	0.775(0.464)	0.016(0.013)	0.000(0.000)					
(III) 60/60/400		Ridge	6.174(0.738)	2.221(0.579)	0.961(0.012)	0.000(0.000)	6.280(0.744)	2.235(0.551)	0.958(0.012)	0.000(0.000)		6.280(0.744)	2.235(0.551)	0.958(0.012)	0.000(0.000)				
	Lasso	7.541(1.227)	0.940(0.335)	0.036(0.016)	0.125(0.070)	5.786(1.224)	1.248(0.669)	0.024(0.015)	0.051(0.058)		5.786(1.224)	1.248(0.669)	0.024(0.015)	0.051(0.058)					
	Alasso	8.708(1.405)	0.682(0.232)	0.036(0.015)	0.171(0.071)	6.504(1.152)	0.960(0.365)	0.022(0.012)	0.085(0.063)		6.504(1.152)	0.960(0.365)	0.022(0.012)	0.085(0.063)					
	Enet	4.739(0.674)	3.559(1.181)	0.204(0.056)	0.000(0.000)	5.358(0.894)	3.756(1.477)	0.198(0.043)	0.001(0.009)		5.358(0.894)	3.756(1.477)	0.198(0.043)	0.001(0.009)					
	SRL	7.423(1.205)	0.897(0.362)	0.039(0.019)	0.120(0.066)	5.647(1.163)	1.174(0.579)	0.029(0.020)	0.040(0.057)		5.647(1.163)	1.174(0.579)	0.029(0.020)	0.040(0.057)					
	SRIG-o	2.489(0.426)	0.761(0.374)	0.005(0.008)	0.000(0.000)	3.245(0.700)	1.303(0.703)	0.001(0.004)	0.000(0.000)		3.245(0.700)	1.303(0.703)	0.001(0.004)	0.000(0.000)					
	SRIG	2.259(0.446)	0.721(0.383)	0.005(0.008)	0.000(0.000)	2.656(0.562)	0.743(0.430)	0.004(0.006)	0.000(0.000)		2.656(0.562)	0.743(0.430)	0.004(0.006)	0.000(0.000)					
	GSRE-o	2.109(0.313)	0.381(0.188)	0.008(0.011)	0.000(0.000)	2.453(0.442)	0.452(0.229)	0.008(0.010)	0.000(0.000)		2.453(0.442)	0.452(0.229)	0.008(0.010)	0.000(0.000)					
	GSRE	2.016(0.317)	0.377(0.185)	0.009(0.010)	0.000(0.000)	2.420(0.448)	0.443(0.224)	0.008(0.010)	0.000(0.000)		2.420(0.448)	0.443(0.224)	0.008(0.010)	0.000(0.000)					

Table 2: Performance comparison of estimation, prediction and model selection for Example 1&2 with t distribution noise.

		Example 1							Example 2						
		$L_2$ distance	RPE	FPR	FNR	$L_2$ distance	RPE	FPR	FNR	$L_2$ distance	RPE	FPR	FNR		
(I)	20/20/400	Ridge	8.191(0.722)	7.175(2.487)	0.967(0.012)	0.000(0.000)	8.836(0.616)	7.774(2.098)	0.966(0.014)	0.000(0.000)	8.836(0.616)	7.774(2.098)	0.966(0.014)	0.000(0.000)	
		Lasso	12.751(1.752)	4.356(3.484)	0.094(0.023)	0.504(0.113)	11.259(1.153)	6.126(3.125)	0.093(0.023)	0.501(0.124)	11.259(1.153)	6.126(3.125)	0.093(0.023)	0.501(0.124)	
		Alasso	12.334(1.762)	3.310(2.229)	0.082(0.020)	0.436(0.105)	11.172(1.484)	5.296(2.938)	0.082(0.022)	0.445(0.130)	11.172(1.484)	5.296(2.938)	0.082(0.022)	0.445(0.130)	
		Enet	6.907(1.215)	5.497(2.813)	0.430(0.043)	0.007(0.020)	8.110(1.035)	6.943(2.481)	0.430(0.050)	0.033(0.066)	8.110(1.035)	6.943(2.481)	0.430(0.050)	0.033(0.066)	
		SRL	12.658(1.636)	3.998(2.627)	0.104(0.026)	0.467(0.110)	11.234(1.495)	5.686(3.090)	0.104(0.026)	0.444(0.130)	11.234(1.495)	5.686(3.090)	0.104(0.026)	0.444(0.130)	
		SRIG-o	8.765(0.672)	13.523(2.362)	0.569(0.060)	0.000(0.000)	9.310(0.524)	12.251(1.736)	0.566(0.053)	0.009(0.040)	9.310(0.524)	12.251(1.736)	0.566(0.053)	0.009(0.040)	
		SRIG	8.810(0.662)	13.683(2.361)	0.571(0.060)	0.000(0.000)	9.232(0.539)	12.053(1.737)	0.564(0.054)	0.009(0.040)	9.232(0.539)	12.053(1.737)	0.564(0.054)	0.009(0.040)	
		GSRE-o	3.528(1.223)	1.827(2.352)	0.023(0.022)	0.000(0.000)	4.714(1.402)	2.668(2.794)	0.026(0.022)	0.013(0.066)	4.714(1.402)	2.668(2.794)	0.026(0.022)	0.013(0.066)	
		GSRE	3.416(1.272)	1.861(2.440)	0.024(0.022)	0.000(0.000)	4.621(1.372)	2.558(2.753)	0.026(0.023)	0.013(0.066)	4.621(1.372)	2.558(2.753)	0.026(0.023)	0.013(0.066)	
		(II)	40/40/400	Ridge	6.985(0.612)	3.544(0.911)	0.962(0.014)	0.000(0.000)	7.345(0.594)	3.850(1.053)	0.964(0.013)	0.000(0.000)	7.345(0.594)	3.850(1.053)	0.964(0.013)
Lasso	9.290(1.360)			1.565(0.671)	0.057(0.020)	0.263(0.086)	7.612(1.374)	2.354(1.268)	0.044(0.017)	0.195(0.101)	7.612(1.374)	2.354(1.268)	0.044(0.017)	0.195(0.101)	
Alasso	9.445(1.394)			1.035(0.441)	0.050(0.021)	0.235(0.090)	7.703(1.568)	1.582(0.840)	0.037(0.014)	0.172(0.088)	7.703(1.568)	1.582(0.840)	0.037(0.014)	0.172(0.088)	
Enet	5.373(0.719)			4.123(1.389)	0.308(0.052)	0.000(0.000)	5.968(0.773)	4.158(1.312)	0.321(0.047)	0.005(0.018)	5.968(0.773)	4.158(1.312)	0.321(0.047)	0.005(0.018)	
SRL	9.194(1.349)			1.459(0.635)	0.067(0.028)	0.240(0.089)	7.446(1.459)	2.229(1.221)	0.052(0.024)	0.172(0.099)	7.446(1.459)	2.229(1.221)	0.052(0.024)	0.172(0.099)	
SRIG-o	3.323(1.039)			1.761(1.494)	0.032(0.051)	0.000(0.000)	4.244(1.466)	2.514(2.179)	0.064(0.085)	0.000(0.000)	4.244(1.466)	2.514(2.179)	0.064(0.085)	0.000(0.000)	
SRIG	3.149(1.073)			1.730(1.455)	0.031(0.053)	0.000(0.000)	3.957(1.307)	2.135(1.852)	0.050(0.073)	0.000(0.000)	3.957(1.307)	2.135(1.852)	0.050(0.073)	0.000(0.000)	
GSRE-o	2.455(0.514)			0.640(0.448)	0.014(0.012)	0.000(0.000)	3.014(0.616)	0.806(0.529)	0.015(0.014)	0.000(0.000)	3.014(0.616)	0.806(0.529)	0.015(0.014)	0.000(0.000)	
GSRE	2.370(0.544)			0.652(0.476)	0.013(0.010)	0.000(0.000)	3.193(0.785)	1.109(0.908)	0.014(0.012)	0.000(0.000)	3.193(0.785)	1.109(0.908)	0.014(0.012)	0.000(0.000)	
(III)	60/60/400			Ridge	6.196(0.733)	2.211(0.599)	0.961(0.015)	0.000(0.000)	6.350(0.748)	2.267(0.624)	0.961(0.014)	0.000(0.000)	6.350(0.748)	2.267(0.624)	0.961(0.014)
		Lasso	7.443(1.239)	0.930(0.403)	0.035(0.016)	0.121(0.073)	5.743(1.231)	1.253(0.730)	0.023(0.014)	0.048(0.065)	5.743(1.231)	1.253(0.730)	0.023(0.014)	0.048(0.065)	
		Alasso	8.456(1.316)	0.658(0.223)	0.035(0.016)	0.167(0.069)	6.482(1.164)	0.961(0.423)	0.023(0.014)	0.080(0.067)	6.482(1.164)	0.961(0.423)	0.023(0.014)	0.080(0.067)	
		Enet	4.679(0.742)	3.452(1.313)	0.210(0.060)	0.000(0.000)	5.316(0.985)	3.687(1.664)	0.203(0.057)	0.001(0.009)	5.316(0.985)	3.687(1.664)	0.203(0.057)	0.001(0.009)	
		SRL	7.900(1.302)	0.991(0.561)	0.262(0.095)	0.103(0.085)	6.216(1.283)	1.347(0.951)	0.198(0.133)	0.029(0.080)	6.216(1.283)	1.347(0.951)	0.198(0.133)	0.029(0.080)	
		SRIG-o	2.482(0.407)	0.759(0.360)	0.004(0.007)	0.000(0.000)	2.774(0.615)	0.813(0.540)	0.002(0.006)	0.000(0.000)	2.774(0.615)	0.813(0.540)	0.002(0.006)	0.000(0.000)	
		SRIG	2.266(0.428)	0.724(0.370)	0.004(0.007)	0.000(0.000)	2.664(0.628)	0.764(0.528)	0.003(0.006)	0.000(0.000)	2.664(0.628)	0.764(0.528)	0.003(0.006)	0.000(0.000)	
		GSRE-o	2.109(0.320)	0.358(0.193)	0.014(0.014)	0.000(0.000)	2.434(0.491)	0.450(0.287)	0.007(0.009)	0.000(0.000)	2.434(0.491)	0.450(0.287)	0.007(0.009)	0.000(0.000)	
		GSRE	2.017(0.324)	0.350(0.187)	0.013(0.014)	0.000(0.000)	2.408(0.480)	0.438(0.263)	0.007(0.010)	0.000(0.000)	2.408(0.480)	0.438(0.263)	0.007(0.010)	0.000(0.000)	

Table 3: Performance comparison of estimation, prediction and model selection for Example 1&2 with laplace distribution noise.

Example 1										Example 2									
	$L_2$ distance	RPE	FPR	FNR	$L_2$ distance	RPE	FPR	FNR	FNR	$L_2$ distance	RPE	FPR	FNR	FNR					
(I) 20/20/400	Ridge	8.091(0.739)	7.074(2.383)	0.966(0.014)	0.000(0.000)	8.830(0.575)	7.685(1.974)	0.968(0.015)	0.000(0.000)	8.830(0.575)	7.685(1.974)	0.968(0.015)	0.000(0.000)	0.000(0.000)					
	Lasso	12.317(1.589)	4.254(3.995)	0.088(0.022)	0.484(0.120)	11.483(1.619)	6.117(3.243)	0.092(0.019)	0.476(0.113)	11.483(1.619)	6.117(3.243)	0.092(0.019)	0.476(0.113)	0.476(0.113)					
	Alasso	12.032(1.558)	3.380(3.020)	0.078(0.022)	0.425(0.117)	11.089(1.610)	5.076(2.782)	0.081(0.023)	0.419(0.112)	11.089(1.610)	5.076(2.782)	0.081(0.023)	0.419(0.112)	0.419(0.112)					
	Enet	6.765(1.326)	5.553(3.003)	0.431(0.055)	0.008(0.029)	8.064(0.996)	6.587(2.399)	0.437(0.044)	0.040(0.079)	8.064(0.996)	6.587(2.399)	0.437(0.044)	0.040(0.079)	0.040(0.079)					
	SRL	12.239(1.581)	3.724(3.096)	0.110(0.028)	0.464(0.113)	11.358(1.755)	5.339(2.379)	0.104(0.029)	0.437(0.105)	11.358(1.755)	5.339(2.379)	0.104(0.029)	0.437(0.105)	0.437(0.105)					
	SRIG-o	8.818(0.639)	13.685(2.280)	0.567(0.069)	0.007(0.047)	9.276(0.545)	12.158(1.759)	0.568(0.062)	0.005(0.023)	9.276(0.545)	12.158(1.759)	0.568(0.062)	0.005(0.023)	0.005(0.023)					
	SRIG	8.869(0.640)	13.866(2.309)	0.568(0.069)	0.007(0.047)	9.205(0.540)	11.978(1.728)	0.567(0.062)	0.005(0.023)	9.205(0.540)	11.978(1.728)	0.567(0.062)	0.005(0.023)	0.005(0.023)					
	GSRE-o	3.233(0.932)	1.363(1.051)	0.026(0.032)	0.000(0.000)	4.437(1.515)	2.242(2.907)	0.026(0.019)	0.015(0.066)	4.437(1.515)	2.242(2.907)	0.026(0.019)	0.015(0.066)	0.015(0.066)					
	GSRE	3.120(0.903)	1.375(1.067)	0.027(0.035)	0.000(0.000)	4.320(1.453)	2.098(2.780)	0.026(0.018)	0.013(0.066)	4.320(1.453)	2.098(2.780)	0.026(0.018)	0.013(0.066)	0.013(0.066)					
	(II) 40/40/400	Ridge	6.801(0.584)	3.635(1.211)	0.963(0.018)	0.000(0.000)	7.351(0.585)	3.835(0.905)	0.965(0.013)	0.000(0.000)	7.351(0.585)	3.835(0.905)	0.965(0.013)	0.000(0.000)	0.000(0.000)				
Lasso		8.939(1.370)	1.641(0.960)	0.050(0.021)	0.227(0.103)	8.017(1.273)	2.531(1.459)	0.045(0.019)	0.203(0.092)	8.017(1.273)	2.531(1.459)	0.045(0.019)	0.203(0.092)	0.203(0.092)					
Alasso		8.954(1.544)	0.996(0.624)	0.039(0.017)	0.193(0.087)	8.252(1.275)	1.863(1.105)	0.039(0.017)	0.187(0.087)	8.252(1.275)	1.863(1.105)	0.039(0.017)	0.187(0.087)	0.187(0.087)					
Enet		5.379(0.826)	4.206(1.560)	0.300(0.046)	0.000(0.000)	5.993(0.821)	4.110(1.471)	0.331(0.053)	0.000(0.000)	5.993(0.821)	4.110(1.471)	0.331(0.053)	0.000(0.000)	0.000(0.000)					
SRL		8.661(1.369)	1.534(0.889)	0.057(0.027)	0.205(0.097)	7.801(1.271)	2.379(1.411)	0.054(0.025)	0.191(0.097)	7.801(1.271)	2.379(1.411)	0.054(0.025)	0.191(0.097)	0.191(0.097)					
SRIG-o		3.239(0.974)	1.641(1.506)	0.023(0.052)	0.000(0.000)	4.340(1.520)	2.643(2.235)	0.075(0.090)	0.000(0.000)	4.340(1.520)	2.643(2.235)	0.075(0.090)	0.000(0.000)	0.000(0.000)					
SRIG		3.039(1.135)	1.644(1.723)	0.022(0.054)	0.000(0.000)	4.208(1.469)	2.496(2.108)	0.072(0.087)	0.000(0.000)	4.208(1.469)	2.496(2.108)	0.072(0.087)	0.000(0.000)	0.000(0.000)					
GSRE-o		2.455(0.502)	0.664(0.498)	0.011(0.014)	0.000(0.000)	3.077(0.744)	0.812(0.634)	0.015(0.017)	0.000(0.000)	3.077(0.744)	0.812(0.634)	0.015(0.017)	0.000(0.000)	0.000(0.000)					
GSRE		2.360(0.550)	0.678(0.515)	0.010(0.013)	0.000(0.000)	3.040(0.738)	0.803(0.622)	0.016(0.017)	0.000(0.000)	3.040(0.738)	0.803(0.622)	0.016(0.017)	0.000(0.000)	0.000(0.000)					
(III) 60/60/400		Ridge	6.041(0.730)	2.095(0.518)	0.963(0.012)	0.000(0.000)	6.419(0.693)	2.326(0.660)	0.961(0.013)	0.000(0.000)	6.419(0.693)	2.326(0.660)	0.961(0.013)	0.000(0.000)	0.000(0.000)				
	Lasso	7.127(1.236)	0.920(0.357)	0.031(0.015)	0.115(0.080)	6.000(0.996)	1.332(0.648)	0.028(0.016)	0.067(0.065)	6.000(0.996)	1.332(0.648)	0.028(0.016)	0.067(0.065)	0.067(0.065)					
	Alasso	7.888(1.435)	0.606(0.279)	0.032(0.018)	0.143(0.090)	6.589(1.155)	0.972(0.391)	0.024(0.016)	0.087(0.068)	6.589(1.155)	0.972(0.391)	0.024(0.016)	0.087(0.068)	0.087(0.068)					
	Enet	4.727(0.803)	3.612(1.374)	0.197(0.054)	0.000(0.000)	5.402(0.896)	3.800(1.379)	0.196(0.046)	0.000(0.000)	5.402(0.896)	3.800(1.379)	0.196(0.046)	0.000(0.000)	0.000(0.000)					
	SRL	7.069(1.254)	0.879(0.357)	0.036(0.018)	0.103(0.084)	5.812(1.041)	1.223(0.573)	0.033(0.021)	0.053(0.056)	5.812(1.041)	1.223(0.573)	0.033(0.021)	0.053(0.056)	0.053(0.056)					
	SRIG-o	2.489(0.423)	0.781(0.344)	0.003(0.006)	0.000(0.000)	2.875(0.534)	0.856(0.463)	0.004(0.007)	0.000(0.000)	2.875(0.534)	0.856(0.463)	0.004(0.007)	0.000(0.000)	0.000(0.000)					
	SRIG	2.281(0.401)	0.748(0.322)	0.003(0.006)	0.000(0.000)	2.772(0.549)	0.808(0.448)	0.004(0.007)	0.000(0.000)	2.772(0.549)	0.808(0.448)	0.004(0.007)	0.000(0.000)	0.000(0.000)					
	GSRE-o	2.127(0.356)	0.400(0.201)	0.010(0.012)	0.000(0.000)	2.574(0.419)	0.505(0.269)	0.008(0.010)	0.000(0.000)	2.574(0.419)	0.505(0.269)	0.008(0.010)	0.000(0.000)	0.000(0.000)					
	GSRE	2.047(0.337)	0.394(0.196)	0.010(0.012)	0.000(0.000)	2.544(0.420)	0.504(0.265)	0.008(0.010)	0.000(0.000)	2.544(0.420)	0.504(0.265)	0.008(0.010)	0.000(0.000)	0.000(0.000)					

Table 4: Performance comparison of estimation, prediction and model selection for Example 1&2 with uniform distribution noise.

Example 1										Example 2									
	$L_2$ distance	RPE	FPR	FNR	$L_2$ distance	RPE	FPR	FNR	FNR	$L_2$ distance	RPE	FPR	FNR	FNR					
(I) 20/20/400	Ridge	8.130(0.745)	7.266(2.614)	0.968(0.015)	0.001(0.009)	8.830(0.588)	7.580(2.125)	0.971(0.013)	0.007(0.024)	8.830(0.588)	7.580(2.125)	0.971(0.013)	0.007(0.024)	0.007(0.024)					
	Lasso	12.460(1.422)	4.432(4.073)	0.092(0.023)	0.485(0.121)	11.528(1.547)	6.079(3.241)	0.092(0.021)	0.481(0.130)	11.528(1.547)	6.079(3.241)	0.092(0.021)	0.481(0.130)	0.481(0.130)					
	Alasso	12.401(1.626)	3.546(3.249)	0.086(0.023)	0.467(0.126)	11.187(1.704)	5.231(3.177)	0.079(0.024)	0.433(0.131)	11.187(1.704)	5.231(3.177)	0.079(0.024)	0.433(0.131)	0.433(0.131)					
	Enet	6.852(1.315)	5.624(3.094)	0.431(0.054)	0.011(0.037)	8.073(1.028)	6.625(2.472)	0.433(0.047)	0.043(0.076)	8.073(1.028)	6.625(2.472)	0.433(0.047)	0.043(0.076)	0.043(0.076)					
	SRL	12.744(1.382)	3.982(3.170)	0.110(0.026)	0.472(0.113)	11.317(1.631)	5.299(2.578)	0.104(0.030)	0.444(0.119)	11.317(1.631)	5.299(2.578)	0.104(0.030)	0.444(0.119)	0.444(0.119)					
	SRIG-o	8.816(0.652)	13.680(2.313)	0.570(0.072)	0.007(0.047)	9.287(0.545)	12.187(1.757)	0.563(0.067)	0.005(0.023)	9.287(0.545)	12.187(1.757)	0.563(0.067)	0.005(0.023)	0.005(0.023)					
	SRIG	8.859(0.658)	13.837(2.352)	0.572(0.069)	0.007(0.047)	9.219(0.545)	12.016(1.741)	0.560(0.067)	0.005(0.023)	9.219(0.545)	12.016(1.741)	0.560(0.067)	0.005(0.023)	0.005(0.023)					
	GSRE-o	3.491(1.099)	1.755(1.540)	0.021(0.026)	0.000(0.000)	4.451(1.435)	2.222(2.600)	0.030(0.023)	0.013(0.066)	4.451(1.435)	2.222(2.600)	0.030(0.023)	0.013(0.066)	0.013(0.066)					
	GSRE	3.337(1.051)	1.674(1.471)	0.025(0.030)	0.000(0.000)	4.397(1.424)	2.194(2.586)	0.028(0.024)	0.013(0.066)	4.397(1.424)	2.194(2.586)	0.028(0.024)	0.013(0.066)	0.013(0.066)					
	(II) 40/40/400	Ridge	6.979(0.531)	3.544(1.024)	0.969(0.010)	0.000(0.000)	7.356(0.488)	3.661(0.884)	0.967(0.012)	0.000(0.000)	7.356(0.488)	3.661(0.884)	0.967(0.012)	0.000(0.000)	0.000(0.000)				
Lasso		9.248(1.365)	1.712(0.923)	0.057(0.020)	0.252(0.097)	7.915(1.254)	2.397(1.164)	0.045(0.019)	0.201(0.095)	7.915(1.254)	2.397(1.164)	0.045(0.019)	0.201(0.095)	0.201(0.095)					
Alasso		9.360(1.335)	1.061(0.540)	0.043(0.017)	0.209(0.077)	8.142(1.318)	1.750(1.076)	0.040(0.016)	0.189(0.075)	8.142(1.318)	1.750(1.076)	0.040(0.016)	0.189(0.075)	0.189(0.075)					
Enet		5.418(0.767)	4.217(1.431)	0.306(0.046)	0.000(0.000)	5.965(0.763)	4.127(1.346)	0.327(0.049)	0.000(0.000)	5.965(0.763)	4.127(1.346)	0.327(0.049)	0.000(0.000)	0.000(0.000)					
SRL		9.095(1.487)	1.566(0.863)	0.063(0.026)	0.233(0.090)	7.658(1.193)	2.223(1.228)	0.048(0.020)	0.176(0.086)	7.658(1.193)	2.223(1.228)	0.048(0.020)	0.176(0.086)	0.176(0.086)					
SRIG-o		3.415(1.105)	1.903(1.751)	0.030(0.053)	0.000(0.000)	4.347(1.428)	2.617(2.068)	0.076(0.096)	0.000(0.000)	4.347(1.428)	2.617(2.068)	0.076(0.096)	0.000(0.000)	0.000(0.000)					
SRIG		3.170(1.175)	1.804(1.767)	0.029(0.053)	0.000(0.000)	4.117(1.320)	2.325(1.877)	0.064(0.089)	0.000(0.000)	4.117(1.320)	2.325(1.877)	0.064(0.089)	0.000(0.000)	0.000(0.000)					
GSRE-o		2.522(0.537)	0.712(0.553)	0.012(0.013)	0.000(0.000)	2.998(0.616)	0.738(0.530)	0.013(0.015)	0.000(0.000)	2.998(0.616)	0.738(0.530)	0.013(0.015)	0.000(0.000)	0.000(0.000)					
GSRE		2.426(0.572)	0.704(0.564)	0.013(0.014)	0.000(0.000)	2.952(0.598)	0.722(0.512)	0.012(0.015)	0.000(0.000)	2.952(0.598)	0.722(0.512)	0.012(0.015)	0.000(0.000)	0.000(0.000)					
(III) 60/60/400		Ridge	6.190(0.657)	2.164(0.515)	0.960(0.014)	0.000(0.000)	6.359(0.695)	2.335(0.731)	0.963(0.010)	0.000(0.000)	6.359(0.695)	2.335(0.731)	0.963(0.010)	0.000(0.000)	0.000(0.000)				
	Lasso	7.456(1.232)	0.972(0.341)	0.036(0.017)	0.132(0.080)	5.922(1.064)	1.294(0.707)	0.028(0.016)	0.068(0.065)	5.922(1.064)	1.294(0.707)	0.028(0.016)	0.068(0.065)	0.068(0.065)					
	Alasso	8.237(1.195)	0.644(0.224)	0.036(0.015)	0.168(0.074)	6.580(1.087)	0.990(0.482)	0.023(0.012)	0.092(0.070)	6.580(1.087)	0.990(0.482)	0.023(0.012)	0.092(0.070)	0.092(0.070)					
	Enet	4.754(0.783)	3.651(1.340)	0.196(0.052)	0.000(0.000)	5.354(1.007)	3.756(1.610)	0.199(0.053)	0.001(0.009)	5.354(1.007)	3.756(1.610)	0.199(0.053)	0.001(0.009)	0.001(0.009)					
	SRL	7.362(1.143)	0.913(0.306)	0.040(0.020)	0.121(0.078)	5.809(1.026)	1.251(0.623)	0.030(0.018)	0.059(0.057)	5.809(1.026)	1.251(0.623)	0.030(0.018)	0.059(0.057)	0.059(0.057)					
	SRIG-o	2.503(0.429)	0.782(0.336)	0.003(0.005)	0.000(0.000)	2.874(0.565)	0.863(0.521)	0.004(0.007)	0.000(0.000)	2.874(0.565)	0.863(0.521)	0.004(0.007)	0.000(0.000)	0.000(0.000)					
	SRIG	2.311(0.399)	0.755(0.321)	0.003(0.005)	0.000(0.000)	2.761(0.575)	0.805(0.498)	0.004(0.008)	0.000(0.000)	2.761(0.575)	0.805(0.498)	0.004(0.008)	0.000(0.000)	0.000(0.000)					
	GSRE-o	2.152(0.366)	0.410(0.181)	0.010(0.010)	0.000(0.000)	2.540(0.416)	0.472(0.271)	0.009(0.012)	0.000(0.000)	2.540(0.416)	0.472(0.271)	0.009(0.012)	0.000(0.000)	0.000(0.000)					
	GSRE	2.082(0.348)	0.402(0.184)	0.011(0.012)	0.000(0.000)	2.507(0.426)	0.464(0.270)	0.009(0.011)	0.000(0.000)	2.507(0.426)	0.464(0.270)	0.009(0.011)	0.000(0.000)	0.000(0.000)					

Table 5: Performance comparison of estimation, prediction and model selection for Example 3 with normal distribution noise.

		$L_2$ distance	RPE	FPR	FNR
(I) 20/20/400	Ridge	9.229 (0.688)	7.278 (1.696)	0.963 (0.016)	0.005 (0.018)
	Lasso	11.060 (1.308)	6.902 (2.401)	0.093 (0.020)	0.508 (0.125)
	Alasso	10.931 (1.282)	6.352 (2.383)	0.084 (0.023)	0.468 (0.127)
	Enet	8.831 (0.971)	6.781 (1.958)	0.412 (0.043)	0.111 (0.105)
	SRL	10.872 (1.471)	6.471 (2.510)	0.171 (0.027)	0.392 (0.150)
	SRIG-o	10.396 (0.383)	11.385 (1.172)	0.846 (0.073)	0.020 (0.051)
	SRIG	9.811 (0.514)	9.960 (1.353)	0.912 (0.041)	0.011 (0.031)
	GSRE-o	7.039 (1.580)	4.199 (2.615)	0.288 (0.109)	0.052 (0.110)
	GSRE	6.145 (1.487)	3.121 (2.296)	0.321 (0.118)	0.025 (0.080)
(II) 40/40/400	Ridge	7.667 (0.563)	3.791 (1.027)	0.960 (0.017)	0.000 (0.000)
	Lasso	7.668 (1.052)	2.859 (1.093)	0.049 (0.018)	0.197 (0.087)
	Alasso	7.825 (1.161)	2.195 (0.919)	0.043 (0.016)	0.205 (0.079)
	Enet	6.959 (0.752)	4.416 (1.170)	0.306 (0.048)	0.019 (0.040)
	SRL	7.513 (1.127)	2.674 (1.052)	0.056 (0.025)	0.176 (0.087)
	SRIG-o	10.263 (0.281)	11.230 (1.061)	0.495 (0.095)	0.009 (0.027)
	SRIG	9.583 (0.440)	9.706 (1.208)	0.589 (0.117)	0.001 (0.009)
	GSRE-o	5.631 (1.318)	2.874 (1.971)	0.040 (0.037)	0.013 (0.040)
	GSRE	4.861 (1.354)	2.074 (1.915)	0.031 (0.022)	0.007 (0.034)
(III) 60/60/400	Ridge	6.839 (0.687)	2.325 (0.511)	0.959 (0.011)	0.000 (0.000)
	Lasso	5.825 (1.062)	1.628 (0.720)	0.044 (0.022)	0.073 (0.075)
	Alasso	6.159 (1.073)	1.208 (0.458)	0.026 (0.017)	0.091 (0.076)
	Enet	6.821 (0.895)	4.644 (1.253)	0.190 (0.056)	0.012 (0.032)
	SRL	5.738 (1.101)	1.625 (0.750)	0.042 (0.025)	0.068 (0.072)
	SRIG-o	4.973 (0.896)	2.253 (0.958)	0.027 (0.017)	0.000 (0.000)
	SRIG	4.207 (0.789)	1.468 (0.705)	0.042 (0.019)	0.000 (0.000)
	GSRE-o	4.093 (0.957)	1.301 (0.784)	0.029 (0.024)	0.001 (0.009)
	GSRE	3.835 (0.814)	1.124 (0.633)	0.026 (0.018)	0.000 (0.000)

Table 6: Performance comparison of estimation, prediction and model selection for Example 3 with t distribution noise.

		$L_2$ distance	RPE	FPR	FNR
(I) 20/20/400	Ridge	9.225 (0.700)	7.231 (1.661)	0.960 (0.014)	0.007 (0.020)
	Lasso	10.969 (1.269)	6.812 (2.440)	0.094 (0.018)	0.509 (0.112)
	Alasso	10.993 (1.239)	6.464 (2.420)	0.086 (0.022)	0.476 (0.123)
	Enet	8.842 (0.980)	6.792 (1.962)	0.416 (0.044)	0.125 (0.117)
	SRL	10.737 (1.373)	6.420 (2.527)	0.173 (0.027)	0.383 (0.154)
	SRIG-o	10.397 (0.390)	11.387 (1.191)	0.839 (0.098)	0.027 (0.075)
	SRIG	9.823 (0.508)	9.980 (1.356)	0.915 (0.040)	0.016 (0.051)
	GSRE-o	6.953 (1.613)	4.088 (2.599)	0.289 (0.102)	0.051 (0.107)
	GSRE	6.177 (1.608)	3.240 (2.432)	0.317 (0.116)	0.023 (0.071)
(II) 40/40/400	Ridge	7.625 (0.606)	3.650 (0.952)	0.963 (0.013)	0.000 (0.000)
	Lasso	7.635 (1.138)	2.832 (1.166)	0.050 (0.019)	0.193 (0.096)
	Alasso	7.707 (1.349)	2.156 (1.001)	0.046 (0.019)	0.193 (0.103)
	Enet	6.968 (0.793)	4.426 (1.238)	0.306 (0.049)	0.021 (0.044)
	SRL	7.539 (1.224)	2.707 (1.168)	0.057 (0.024)	0.175 (0.096)
	SRIG-o	10.262 (0.289)	11.230 (1.078)	0.496 (0.105)	0.008 (0.026)
	SRIG	9.518 (0.550)	9.579 (1.412)	0.583 (0.146)	0.001 (0.009)
	GSRE-o	5.626 (1.393)	2.881 (2.003)	0.039 (0.028)	0.015 (0.041)
	GSRE	4.714 (1.007)	1.803 (1.089)	0.033 (0.026)	0.000 (0.000)
(III) 60/60/400	Ridge	6.925 (0.752)	2.341 (0.577)	0.962 (0.012)	0.000 (0.000)
	Lasso	5.864 (1.131)	1.657 (0.742)	0.040 (0.023)	0.077 (0.081)
	Alasso	6.138 (1.175)	1.205 (0.537)	0.026 (0.015)	0.087 (0.070)
	Enet	6.873 (0.847)	4.703 (1.232)	0.188 (0.051)	0.013 (0.036)
	SRL	5.737 (1.135)	1.600 (0.717)	0.044 (0.025)	0.075 (0.073)
	SRIG-o	4.963 (0.866)	2.233 (0.905)	0.026 (0.022)	0.000 (0.000)
	SRIG	4.188 (0.771)	1.439 (0.671)	0.040 (0.013)	0.000 (0.000)
	GSRE-o	4.018 (0.813)	1.198 (0.590)	0.034 (0.025)	0.001 (0.009)
	GSRE	3.782 (0.745)	1.060 (0.545)	0.030 (0.018)	0.000 (0.000)

Table 7: Performance comparison of estimation, prediction and model selection for Example 3 with laplace distribution noise.

		$L_2$ distance	RPE	FPR	FNR
(I) 20/20/400	Ridge	9.188 (0.634)	7.307 (1.556)	0.962 (0.015)	0.007 (0.020)
	Lasso	10.950 (1.347)	6.687 (2.558)	0.093 (0.022)	0.512 (0.118)
	Alasso	10.911 (1.484)	6.328 (2.830)	0.086 (0.021)	0.465 (0.134)
	Enet	8.800 (0.957)	6.712 (1.886)	0.401 (0.047)	0.103 (0.101)
	SRL	10.647 (1.492)	6.193 (2.783)	0.170 (0.029)	0.399 (0.161)
	SRIG-o	10.386 (0.337)	11.350 (1.039)	0.836 (0.068)	0.017 (0.038)
	SRIG	9.809 (0.481)	9.939 (1.263)	0.909 (0.052)	0.011 (0.034)
	GSRE-o	6.891 (1.680)	3.975 (2.583)	0.260 (0.104)	0.045 (0.101)
	GSRE	6.048 (1.504)	3.015 (2.157)	0.299 (0.122)	0.016 (0.061)
(II) 40/40/400	Ridge	7.527 (0.634)	3.646 (1.012)	0.960 (0.017)	0.000 (0.000)
	Lasso	7.398 (1.056)	2.685 (1.168)	0.049 (0.019)	0.185 (0.101)
	Alasso	7.195 (1.161)	1.854 (0.800)	0.040 (0.019)	0.151 (0.100)
	Enet	6.874 (0.815)	4.327 (1.202)	0.303 (0.056)	0.013 (0.033)
	SRL	7.129 (0.957)	2.412 (1.005)	0.059 (0.026)	0.151 (0.091)
	SRIG-o	10.259 (0.289)	11.221 (1.062)	0.504 (0.086)	0.011 (0.028)
	SRIG	9.571 (0.467)	9.684 (1.265)	0.593 (0.108)	0.004 (0.021)
	GSRE-o	5.359 (1.264)	2.543 (1.541)	0.035 (0.028)	0.012 (0.032)
	GSRE	4.346 (1.185)	1.555 (1.197)	0.033 (0.028)	0.000 (0.000)
(III) 60/60/400	Ridge	6.645 (0.714)	2.170 (0.474)	0.959 (0.015)	0.000 (0.000)
	Lasso	5.479 (1.159)	1.478 (0.677)	0.041 (0.019)	0.063 (0.078)
	Alasso	5.654 (1.263)	1.037 (0.450)	0.024 (0.014)	0.071 (0.065)
	Enet	6.669 (0.931)	4.419 (1.363)	0.187 (0.047)	0.005 (0.018)
	SRL	5.326 (1.072)	1.353 (0.560)	0.047 (0.026)	0.047 (0.062)
	SRIG-o	4.866 (0.716)	2.115 (0.753)	0.025 (0.016)	0.000 (0.000)
	SRIG	3.999 (0.605)	1.280 (0.538)	0.041 (0.008)	0.000 (0.000)
	GSRE-o	3.750 (0.671)	1.016 (0.450)	0.034 (0.023)	0.000 (0.000)
	GSRE	3.524 (0.639)	0.890 (0.428)	0.028 (0.017)	0.000 (0.000)

Table 8: Performance comparison of estimation, prediction and model selection for Example 3 with uniform distribution noise.

		$L_2$ distance	RPE	FPR	FNR
(I) 20/20/400	Ridge	9.235 (0.635)	7.242 (1.596)	0.965 (0.014)	0.004 (0.016)
	Lasso	11.223 (1.375)	6.974 (2.660)	0.095 (0.022)	0.528 (0.125)
	Alasso	11.030 (1.505)	6.383 (2.996)	0.091 (0.023)	0.487 (0.136)
	Enet	8.867 (0.967)	6.761 (1.906)	0.410 (0.052)	0.107 (0.097)
	SRL	10.934 (1.337)	6.374 (2.637)	0.168 (0.030)	0.420 (0.160)
	SRIG-o	10.386 (0.339)	11.342 (1.038)	0.845 (0.070)	0.021 (0.044)
	SRIG	9.817 (0.478)	9.938 (1.246)	0.908 (0.050)	0.015 (0.036)
	GSRE-o	7.045 (1.627)	4.148 (2.630)	0.271 (0.109)	0.056 (0.105)
	GSRE	6.253 (1.542)	3.297 (2.353)	0.298 (0.119)	0.020 (0.074)
(II) 40/40/400	Ridge	7.613 (0.545)	3.755 (1.062)	0.960 (0.012)	0.000 (0.000)
	Lasso	7.582 (0.884)	2.775 (1.029)	0.054 (0.022)	0.187 (0.086)
	Alasso	7.546 (0.995)	2.077 (0.830)	0.039 (0.015)	0.172 (0.089)
	Enet	6.924 (0.839)	4.381 (1.315)	0.314 (0.054)	0.017 (0.035)
	SRL	7.334 (0.972)	2.562 (1.028)	0.061 (0.023)	0.153 (0.092)
	SRIG-o	10.282 (0.284)	11.274 (1.056)	0.508 (0.086)	0.012 (0.029)
	SRIG	9.594 (0.490)	9.733 (1.305)	0.602 (0.111)	0.000 (0.000)
	GSRE-o	5.469 (1.250)	2.684 (1.719)	0.035 (0.027)	0.012 (0.032)
	GSRE	4.490 (0.984)	1.628 (0.959)	0.034 (0.030)	0.000 (0.000)
(III) 60/60/400	Ridge	6.717 (0.618)	2.238 (0.460)	0.961 (0.014)	0.000 (0.000)
	Lasso	5.610 (0.919)	1.487 (0.556)	0.047 (0.026)	0.055 (0.061)
	Alasso	6.034 (0.989)	1.178 (0.439)	0.024 (0.012)	0.084 (0.064)
	Enet	6.684 (0.841)	4.430 (1.261)	0.193 (0.054)	0.004 (0.016)
	SRL	5.584 (0.906)	1.465 (0.506)	0.046 (0.025)	0.052 (0.059)
	SRIG-o	4.912 (0.815)	2.170 (0.871)	0.024 (0.012)	0.000 (0.000)
	SRIG	4.010 (0.606)	1.268 (0.515)	0.044 (0.010)	0.000 (0.000)
	GSRE-o	3.899 (0.669)	1.120 (0.514)	0.029 (0.021)	0.000 (0.000)
	GSRE	3.642 (0.692)	0.956 (0.514)	0.028 (0.016)	0.000 (0.000)